fractal and fractional

MDPI

Article

Non-Linear Analysis of Novel Equivalent Circuits of Single-Diode Solar Cell Models with Voltage-Dependent Resistance

Mahendiran Vellingiri [1,2], Muhyaddin Rawa [1,3], Sultan Alghamdi [1,2], Abdullah A. Alhussainy [1,3], Ahmed S. Althobiti [1,3], Martin Calasan [4,*], Mihailo Micev [4], Ziad M. Ali [5,6] and Shady H. E. Abdel Aleem [7]

1 Smart Grids Research Group, Center of Research Excellence in Renewable Energy and Power Systems, King Abdulaziz University, Jeddah 21589, Saudi Arabia
2 Department of Electrical and Computer Engineering, Faculty of Engineering, King Abdulaziz University, Jeddah 21589, Saudi Arabia
3 Department of Electrical and Computer Engineering, Faculty of Engineering, K. A. CARE Energy Research and Innovation Center, King Abdulaziz University, Jeddah 21589, Saudi Arabia
4 Faculty of Electrical Engineering, University of Montenegro, 81000 Podgorica, Montenegro
5 Electrical Engineering Department, College of Engineering, Prince Sattam bin Abdulaziz University, Wadi Addawaser 11991, Saudi Arabia
6 Electrical Engineering Department, Aswan Faculty of Engineering, Aswan University, Aswan 81542, Egypt
7 Department of Electrical Engineering, Valley High Institute of Engineering and Technology, Science Valley Academy, Qalyubia 44971, Egypt
* Correspondence: martinc@ucg.ac.me

Abstract: The most commonly used model of solar cells is the single-diode model, with five unknown parameters. First, this paper proposes three variants of the single-diode model, which imply the voltage dependence of the series resistance, parallel resistance, and both resistors. Second, analytical relationships between the current and the voltage expressed were derived using the Lambert W function for each proposed model. Third, the paper presents a hybrid algorithm, Chaotic Snake Optimization (Chaotic SO), combining chaotic sequences with the snake optimization algorithm. The application of the proposed models and algorithm was justified on two well-known solar photovoltaic (PV) cells—RTC France solar cell and Photowatt-PWP201 module. The results showed that the root-mean-square-error (RMSE) values calculated by applying the proposed equivalent circuit with voltage dependence of both resistors are reduced by 20% for the RTC France solar cell and 40% for the Photowatt-PWP201 module compared to the standard single-diode equivalent circuit. Finally, an experimental investigation was conducted into the applicability of the proposed models to a solar laboratory module, and the results obtained proved the relevance and effectiveness of the proposed models.

Keywords: chaotic snake optimization; Lambert W function; optimization; mathematical models; solar PV cells

Citation: Vellingiri, M.; Rawa, M.; Alghamdi, S.; Alhussainy, A.A.; Althobiti, A.S.; Calasan, M.; Micev, M.; Ali, Z.M.; Aleem, S.H.E.A. Non-Linear Analysis of Novel Equivalent Circuits of Single-Diode Solar Cell Models with Voltage-Dependent Resistance. *Fractal Fract.* **2023**, *7*, 95. https://doi.org/10.3390/fractalfract7010095

Academic Editor: Savin Treanţă

Received: 10 December 2022
Revised: 10 January 2023
Accepted: 11 January 2023
Published: 14 January 2023

1. Introduction

1.1. Background

In the near future, energy demand will almost double for many reasons, while water and food demand is expected to increase significantly. Unfortunately, countries' economies are greatly affected by energy shortages, especially when energy resources are not independent, as evidenced by the Russian-Ukrainian war and the COVID-19 pandemic. Thus, on the one hand, all states aspire to harness their natural resources to serve them and to be economically independent. On the other hand, industrial development and environmental pollution are increasingly affecting the world's decarbonization [1,2]. The use

of renewable energy sources and energy storage technologies can help reduce this pressure on the planet. In this regard, very high expectations and growth in energy use rely on solar energy as a promising player in the carbon-free independent energy mix [3].

In this context, any energy analysis that looks at how a solar power plant connects to the grid has to know how powerful the solar panels are. However, power calculation is directly related to solar power plant management to maximize solar energy, based on the regulation of output voltage and current to obtain maximum power. The knowledge of the solar panel's mathematical model, i.e., its solar cells' electrical properties, is fundamental to understanding the challenges of power regulation of the solar panel or the so-called maximum power point tracking (MPPT) [4]. Because of this, estimating the parameters of solar models while creating new models to represent solar cells' performance is of considerable interest in energy-based research works.

Single-diode, double-diode, and triple-diode models are used in the literature to simulate solar cells electrically. Each of these models consists of a single current generator acting as the source of photocurrent (I_{PV}) and two resistances, R_S and R_P, which are connected in series and parallel, respectively. The number of diodes in an equivalent circuit can be determined using the triple-diode, double-diode, and single-diode models. The electrical parameters of the diodes employed in the triple-diode and double-diode models—the ideal factor (n) and reverse saturation current (I_0)—are different. The traditional single-diode model has five parameters, the double-diode model has seven parameters, and the triple-diode model has nine parameters [5,6].

1.2. Motivation

At the beginning of the 2000s, several works were presented to investigate new equivalent circuits of solar cell models, which have additional resistors and capacitors [5-8]. In addition, in the last few years, several works have also been published in which modified equivalent circuits of solar models have been proposed, where additional resistors are added in series with the diode [7]. Specifically, a modification of the triple-diode equivalent circuit has been proposed in [7], and the single-diode equivalent circuit in [8]. However, based on the presented results in these works, it was clear that the proposed modifications in the equivalent circuits have not significantly improved the estimation accuracy of the solar cell parameters, which represents the main motivation for this research. Therefore, the need for an accurate but simple model of solar cells is still an important and trendy research goal. It should be emphasized that in one-diode models and their modified variants [8], there is an analytical dependence between current and voltage, which is not the case in the double-diode and triple-diode models.

1.3. Methodology

In the literature, the authors in [9] presented a modified single-diode model of solar cells in which the series resistance is represented as a voltage-dependent component. The findings of multiple experiments and techniques for modeling this voltage dependency were provided in the paper. Based on [9], emphasis will be placed on creating a novel model in this study that considers both series and parallel resistance and voltage dependency. The primary cause of this is that it was observed while studying solar cell model designs that their characteristics limit the accurate fitting of the simulated and measured curves at high voltage values.

From the point of view of parameter estimation methods, it can be said that the application of metaheuristic algorithms dominates in scientific publications [10–18]. These algorithms have a straightforward application, fast search, and adaptability for the range of parameter changes. The list of metaheuristic algorithms and the data source is given in the Appendix A in Tables A1 and A2. The mentioned tables describe the algorithms used for estimating the parameters in the literature known as solar cells RTC France and PWP Photowatt cell [19,20]. In addition, classical numerical methods were used to estimate the parameters of solar cells, especially those based on iterative methods. Besides, there are

analytical methods, which, unlike others, involve many approximate solutions and are the least accurate [8]. To sum up, the most efficient model has not yet been found, nor has the approach for estimating the parameters of solar cells. For this reason, a new hybrid variant of a metaheuristic algorithm is proposed in this work. Namely, it was learned from the literature that the hybridization of algorithms supports the speed of convergence and the obtained solutions [8].

1.4. Novelty and Contributions

The single-diode model is modified in three ways in this study, implying that the series resistance, parallel resistance, and both resistances are all voltage-dependent. Analytical relationships between the expressed current and voltage were developed using the Lambert W function for each suggested model. The paper also introduces a hybrid approach called Chaotic Snake Optimization (Chaotic SO), which combines the snake optimization algorithm and chaotic sequences. The application of the proposed models and algorithm was justified on two well-known solar PV cells–RTC France solar cell and Photowatt-PWP201 module. The findings demonstrated that the suggested equivalent circuit with voltage dependency of both series and parallel resistance has much lower root-mean-square-error (RMSE) values than the conventional single-diode equivalent circuit. Finally, experimental research was carried out to see whether the suggested models could be used in a solar laboratory module, and the outcomes demonstrated the adaptability and efficacy of the proposed models.

The primary contributions of this work are briefed as follows:

- Three new variants of the single-diode model of solar cells are proposed.
- The voltage dependence of the series resistance, parallel resistance and both of them are considered.
- Analytical expressions for current-voltage dependences of the proposed solar cell models are derived using the Lambert W function.
- An improved snake optimization algorithm using chaotic sequences is presented in this work for estimating the parameters of the investigated solar cell and module.
- The results of comparing the proposed algorithm and numerous literature-known algorithms are presented.
- An experimental investigation was conducted into the applicability of the proposed models to a solar laboratory module, and the results obtained proved the relevance and effectiveness of the proposed models.

1.5. Organization

The paper was divided into several sections to present the research results better. In Section 2, a mathematical description of the standard single-diode model of solar cells is given, as well as the results of calculating current-voltage characteristics for two literature-known cells whose parameters were determined by applying different optimization methods. In Section 3, new single-diode equivalent circuits of solar cells are proposed, and the analytical relationships of their current and voltage expressions are presented. Section 4 presents a novel hybrid metaheuristic algorithm called chaotic snake optimization (Chaotic SO). Section 5 presents the results of estimating the parameters of the investigated solar cells using the standard and the proposed equivalent circuits. Section 6 presents the experimental results conducted on a laboratory solar cell. The concluding remarks and future research directions are given at the end of the paper in Section 7, followed by the appendices.

2. Single-Diode Solar Cell Model and Discussion of the Related Literature

This section is divided into two subsections—basic information about the standard single-diode solar cell model and a discussion of the related literature review.

2.1. Basic Information about the Standard Single-Diode Solar Cell Model

The standard single-diode solar cell model (SDM) is a commonly used model for solar cell representation [3]. The equivalent circuit of the SDM is explored in Figure 1. In this figure, the labels are given as follows: R_S is the series resistance, R_P is the parallel resistance, I_{pv} represents the photo-generated current, and D is the diode.

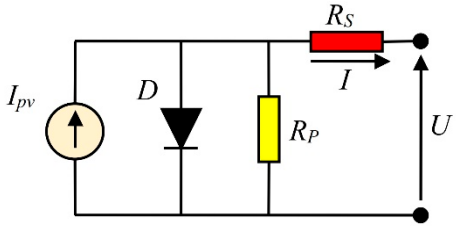

Figure 1. Equivalent circuit of the standard single-diode solar cell model.

The current-voltage relationship of this model is formulated as follows [3]:

$$I = I_{pv} - I_0\left(e^{\frac{U+IR_S}{nV_t}} - 1\right) - \frac{U+IR_S}{R_P} \tag{1}$$

where I is the output current, U denotes the voltage, n is the ideality factor of the diode, and $V_t = K_B T/q$ is the thermal voltage (K_B is the Boltzmann constant, T is the temperature, and q is the electron's charge).

In SDM, the analytical solution for the current as a function of the voltage is given as follows [3]:

$$I = \frac{R_P\left(I_{pv}+I_0\right)-U}{R_S+R_P} - \frac{nV_t}{R_S}W(\beta) \tag{2}$$

so that

$$\beta = \frac{I_0 R_P R_S}{nV_t\left(R_S+R_P\right)}\mathrm{e}^{\frac{R_P\left(R_S I_{pv}+R_S I_0+U\right)}{nV_t\left(R_S+R_P\right)}} \tag{3}$$

where $W(\beta)$ represents the solution of the Lambert W function, a function of the type $W(\beta) = \beta\cdot\exp(-W(\beta))$ that can be solved using several methods. Regarding the analytical solution of this equation, it is evident that the special trans function theory (STFT) is the most efficient and accurate method over other analytical solutions in the available literature [3,5]. Therefore, using the STFT, the analytical closed-form solution for the current has the following form:

$$I = \frac{R_P\left(I_{pv}+I_0\right)-U}{R_S+R_P} - \frac{nV_t\beta}{R_S}\frac{\sum_{k=0}^{M}\frac{\beta^k(M-k)^k}{k!}}{\sum_{k=0}^{M+1}\frac{\beta^k(M+1-k)^k}{k!}}, \tag{4}$$

where M represents a positive integer, and the mathematical genesis of the analytical closed-form solution of the Lambert W function, in addition to the theoretical derivation and proofs, are derived in [21].

2.2. Discussion of the Related Literature Review

Tables A1 and A2 are given in Appendix A, in which a literature review of the estimated parameters using several literature-known approaches that investigated the RTC France solar cell and the Photowatt-PWP201 module are presented. In these tables, values of the root-mean-square-error (RMSE) are calculated as follows:

$$RMSE = \sqrt{\frac{1}{N_{mes}} \sum_{k=1}^{N_{mes}} \left(I_k^{meas} - I_k^{sim} \right)^2} \quad (5)$$

N_{mes} represents the total number of the measured points, while the simulated current values are calculated using (2)–(5). Therefore, this metric defines the degree of matching between measured and simulated curves value. All calculations were carried out in the MATLAB software package, 2018 version.

The graphical presentation of the calculated RMSE values is given in Figure 2a,b for the solar cells investigated. The 3D graph, which illustrates the voltage-method-current and voltage-method-power for both cells, is given in Figures 3–6.

Based on the presented results, it is clear that many methods enable almost the same results (e.g., values of the estimated parameters) and almost equal RMSE values. This remark is also apparent in the presented 3D graphs. The minimum value of RMSE for the RTC France solar cell was provided by Method 204 [13] in Table A1—application of the GAMS program. The minimum value of RMSE for the Photowatt-PWP201 module was provided by Method 43 [13] in Table A2—application of the guaranteed convergence particle swarm optimization (GCPSO). For RTC France solar cell, the minimum RMSE value is $7.730068 \cdot 10^{-4}$, whilst the minimum RMSE value is $2.040452 \cdot 10^{-3}$ for the Photowatt-PWP201 module.

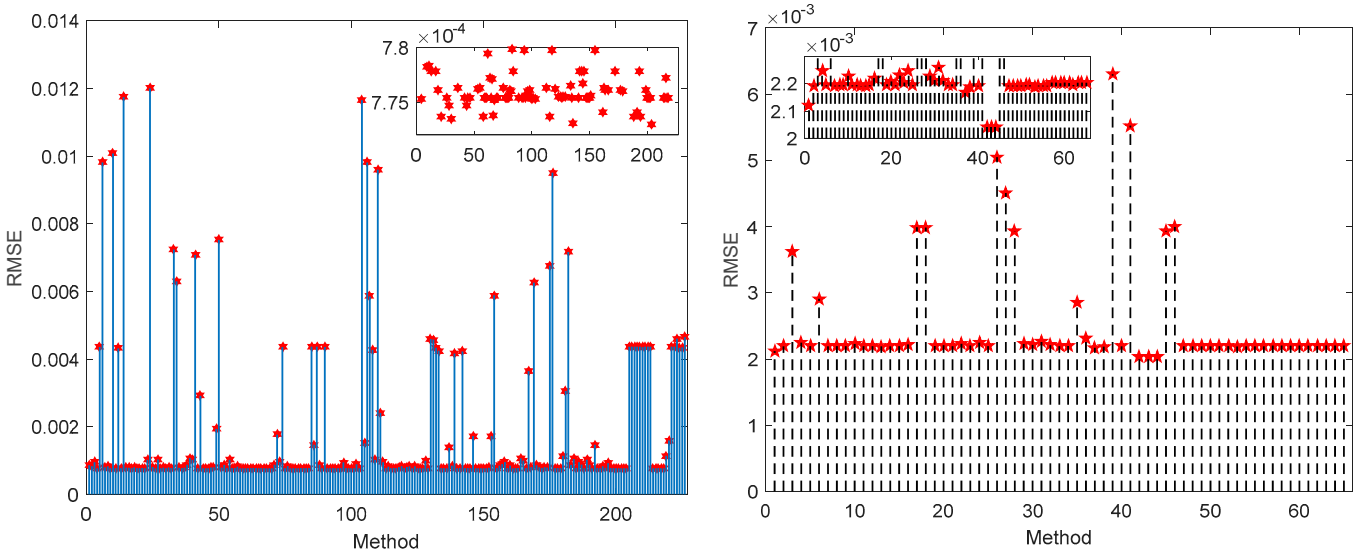

Figure 2. RMSE calculated for: (**a**) RTC France solar cell; (**b**) Photowatt-PWP201 module.

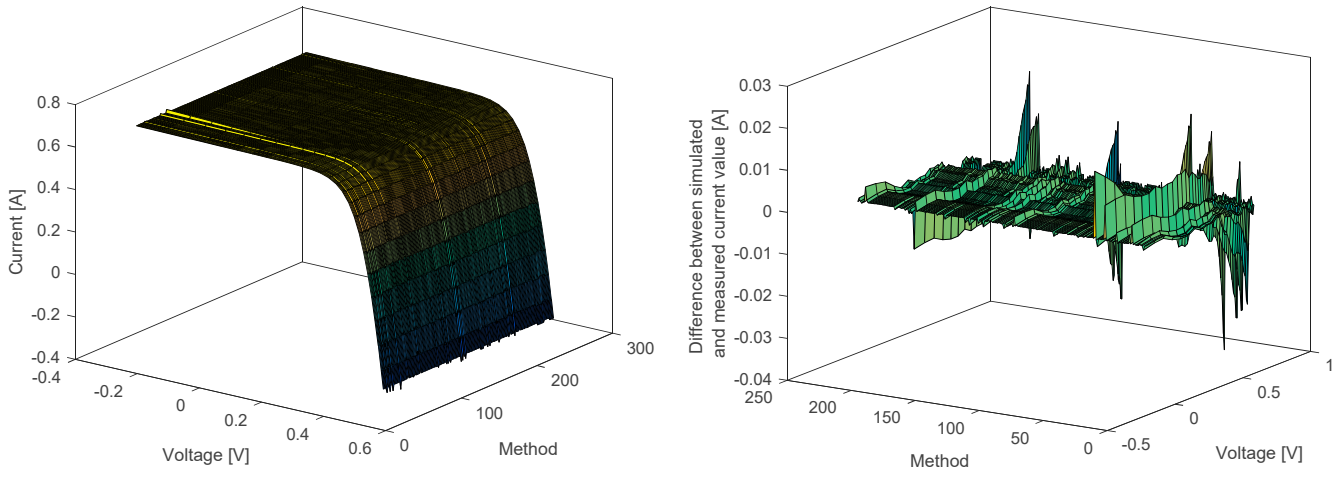

(**a**) (**b**)

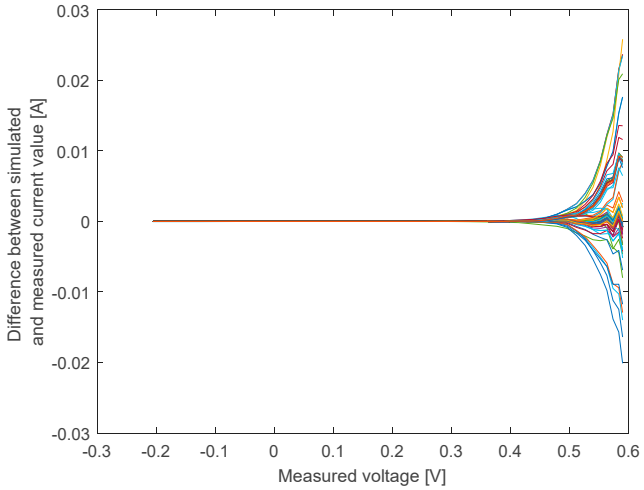

(**c**)

Figure 3. RTC France solar cell: (**a**) current-voltage characteristics; (**b**) the corresponding error; (**c**) error in the current values versus the measured voltage for all methods.

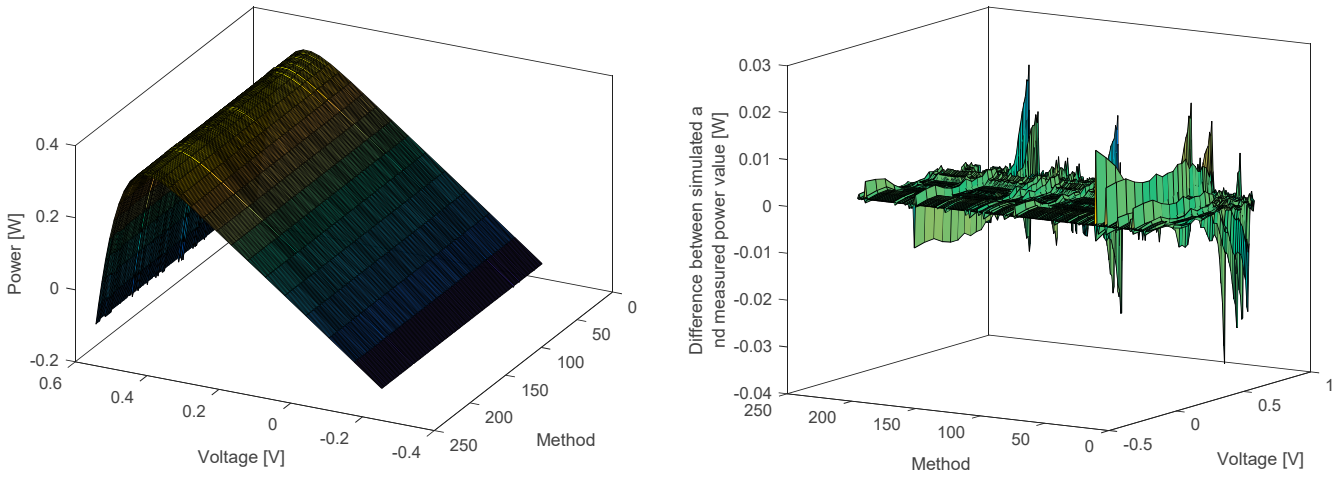

(**a**) (**b**)

Figure 4. RTC France solar cell: (**a**) power-voltage characteristics; (**b**) the corresponding error.

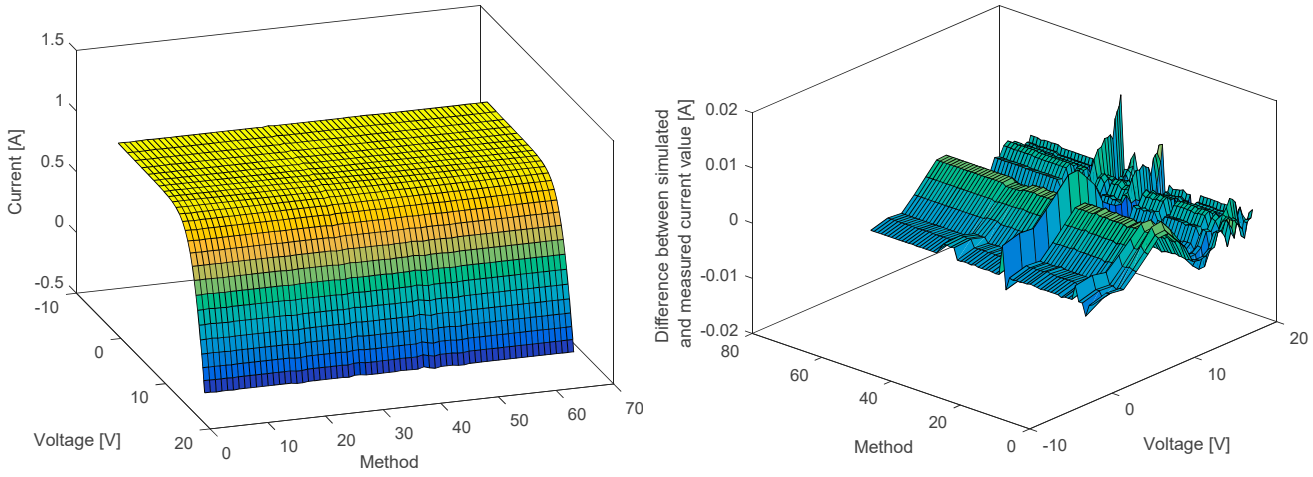

(**a**) (**b**)

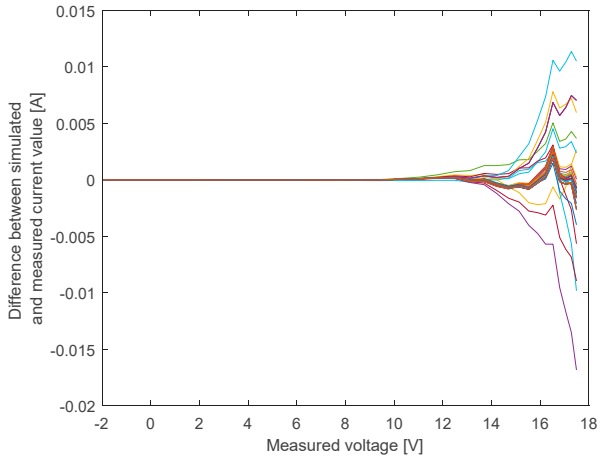

(**c**)

Figure 5. Photowatt-PWP201 module: (**a**) current-voltage characteristics; (**b**) the corresponding error; (**c**) error in the current values versus the measured voltage for all methods.

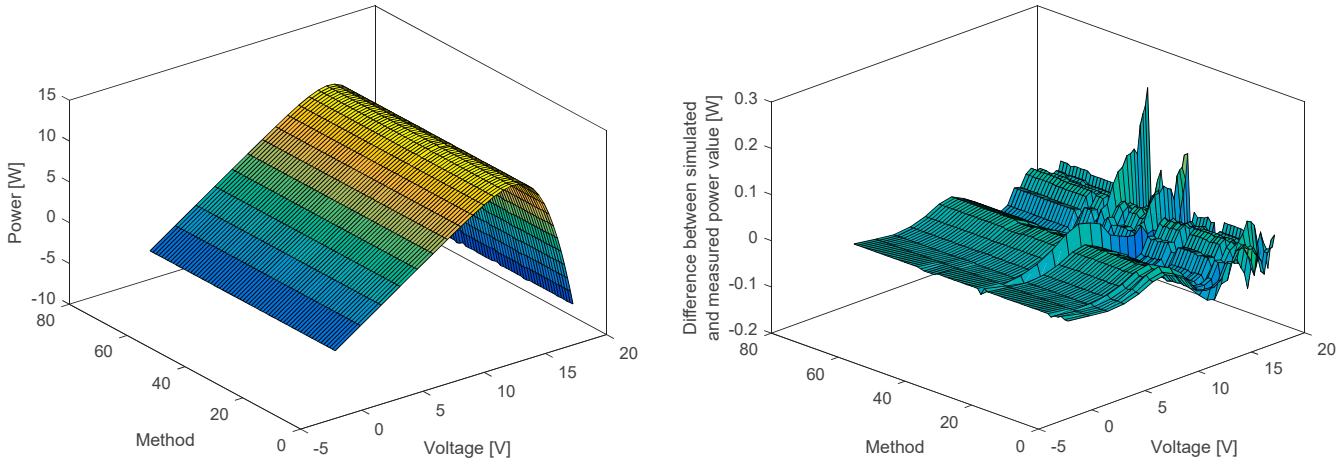

(**a**) (**b**)

Figure 6. Photowatt-PWP201 module: (**a**) power-voltage characteristics; (**b**) the corresponding error.

3. Equivalent Circuits Proposed

The modified SDM with voltage-dependent series resistance was proposed in [9] to elucidate the electrical behavior of organic solar cells while enhancing the modeling accuracy and benefiting from the simplicity of the equivalent circuit. The reasons for introducing the voltage-dependent series resistance and its physical interpretation were described in [9], in which the modification was mainly related to the internal processes of charge extraction and charge transport. Besides, in [9], it was concluded that a voltage-dependent series resistance provides good knowledge about the behavior of the organic solar cells at different applied voltage regions.

Based on [9], in this section, three novel SDM circuits, shown in Figure 7, are proposed. Unlike the standard SDM, these circuits have voltage-dependent series resistance called SDM$_{RS}$ (shown in Figure 7a), voltage-dependent parallel resistance called SDM$_{RP}$ (shown in Figure 7b), and voltage dependence of both resistances called SDM$_{RPRS}$ (shown in Figure 7c).

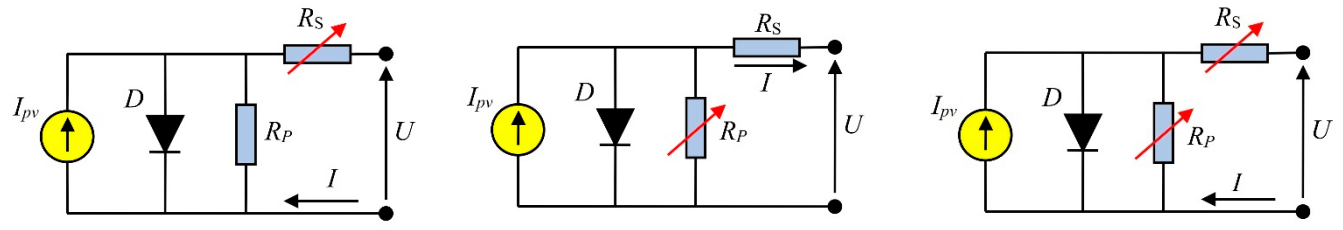

(**a**) (**b**) (**c**)

Figure 7. Proposed equivalent circuit non-linear single diode models of solar cells: (**a**) SDM$_{RS}$; (**b**) SDM$_{RP}$; (**c**) SDM$_{RPRS}$.

In SDM$_{RS}$, the analytical solution for the current (I_{n-R_S}) as a function of the voltage is formulated as follows:

$$I_{n-R_s} = \frac{R_P\left(I_{pv}+I_0\right)-U}{R_{S0}\left(1+k_{n-R_s}U\right)+R_P} - \frac{nV_t}{R_{S0}\left(1+k_{n-R_s}U\right)}W\left(\beta_{n-R_s}\right) \tag{6}$$

where

$$\beta_{n-R_s} = \frac{I_0 R_P R_{S0}\left(1+k_{n-R_s}U\right)}{nV_t\left(R_{S0}\left(1+k_{n-R_s}U\right)+R_P\right)}\mathrm{e}^{\frac{R_P\left(R_{S0}\left(1+k_{n-R_s}U\right)I_{pv}+R_{S0}\left(1+k_{n-R_s}U\right)I_0+U\right)}{nV_t\left(R_{S0}\left(1+k_{n-R_s}U\right)+R_P\right)}} \tag{7}$$

where R_{S0} is the series resistance at zero voltage (Ω), while k_{n-R_s} is the series resistance-voltage coefficient (1/V), applying the STFT [22], the current-voltage expression for this model, derived as follows:

$$I_{n-R_s} = \frac{R_P\left(I_{pv}+I_0\right)-U}{R_{S0}\left(1+k_{n-R_s}U\right)+R_P} - \frac{nV_t\beta_{n-R_s}}{R_{S0}\left(1+k_{n-R_s}U\right)}\left(\frac{\sum_{k=0}^{M}\frac{\beta_{n-R_s}{}^{k}\left(M-k\right)^{k}}{k!}}{\sum_{k=0}^{M+1}\frac{\beta_{n-R_s}{}^{k}\left(M+1-k\right)^{k}}{k!}}\right) \tag{8}$$

In SDM$_{RP}$, the analytical solution for the current (I_{n-R_P}) as a function of the voltage is formulated as follows:

$$I_{n-R_P} = \frac{R_{P0}\left(1+k_{n-R_P}U\right)\left(I_{pv}+I_0\right)-U}{R_S+R_{P0}\left(1+k_{n-R_P}U\right)} - \frac{nV_t}{R_S}W\left(\beta_{n-R_P}\right) \tag{9}$$

where

$$\beta_{n-R_P} = \frac{I_0 R_S R_{P0}\left(1+k_{n-R_P}U\right)}{nV_t\left(R_S+R_{P0}\left(1+k_{n-R_P}U\right)\right)}\mathrm{e}^{\frac{R_{P0}\left(1+k_{n-R_P}U\right)\left(R_S I_{pv}+R_S I_0+U\right)}{nV_t\left(R_S+R_{P0}\left(1+k_{n-R_P}U\right)\right)}} \tag{10}$$

where R_{P0} is the parallel resistance at zero voltage (Ω), while k_{n-R_P} is the parallel resistance-voltage coefficient (1/V), and applying the STFT [22], the current-voltage expression is derived for this model as follows:

$$I_{n-R_P} = \frac{R_{P0}\left(1+k_{n-R_P}U\right)\left(I_{pv}+I_0\right)-U}{R_S+R_{P0}\left(1+k_{n-R_P}U\right)} - \frac{nV_t\beta_{n-R_P}}{R_S}\left(\frac{\sum_{k=0}^{M}\frac{\beta_{n-R_P}{}^{k}\left(M-k\right)^{k}}{k!}}{\sum_{k=0}^{M+1}\frac{\beta_{n-R_P}{}^{k}\left(M+1-k\right)^{k}}{k!}}\right) \tag{11}$$

In SDM$_{RPRS}$, the analytical solution for the current $(I_{n-R_PR_S})$ as a function of the voltage is formulated as follows:

$$I_{n-R_PR_S} = \frac{R_{P0}\left(1+k_{n-R_P}U\right)\left(I_{pv}+I_0\right)-U}{R_{S0}\left(1+k_{n-R_s}U\right)+R_{P0}\left(1+k_{n-R_P}U\right)} - \frac{nV_t}{R_{S0}\left(1+k_{n-R_s}U\right)}W\left(\beta_{n-R_PR_S}\right) \tag{12}$$

where

$$\beta_{n-R_PR_S} = \frac{I_0 R_{S0} R_{P0}\left(1+k_{n-R_P}U\right)\left(1+k_{n-R_s}U\right)}{nV_t\left(R_{S0}\left(1+k_{n-R_s}U\right)+R_{P0}\left(1+k_{n-R_P}U\right)\right)}\mathrm{e}^{\frac{R_{P0}\left(1+k_{n-R_P}U\right)\left(R_{S0}\left(1+k_{n-R_s}U\right)I_{pv}+R_{S0}\left(1+k_{n-R_s}U\right)I_0+U\right)}{nV_t\left(R_{S0}\left(1+k_{n-R_s}U\right)+R_{P0}\left(1+k_{n-R_P}U\right)\right)}} \tag{13}$$

Applying the STFT [22], the current-voltage expression is derived as follows:

$$I_{n-R_P R_S} = \frac{R_{P0}\left(1+k_{n-R_P}U\right)\left(I_{pv}+I_0\right)-U}{R_{S0}\left(1+k_{n-R_s}U\right)+R_{P0}\left(1+k_{n-R_P}U\right)} - \frac{nV_t\beta_{n-R_P R_S}}{R_S}\left(\frac{\sum_{k=0}^{M}\frac{\beta_{n-R_P R_S}{}^{k}\left(M-k\right)^{k}}{k!}}{\sum_{k=0}^{M+1}\frac{\beta_{n-R_P R_S}{}^{k}\left(M+1-k\right)^{k}}{k!}}\right) \quad (14)$$

4. Chaotic SO Algorithm Proposed

The snake optimization (SO) algorithm [23] is inspired by the behavior of snakes, which can be explained in several phases. If the temperature is low and the food is available, the snakes' mating occurs. Otherwise, snakes will search for food or eat the existing food, depending on the remaining quantity of food.

Like all metaheuristic algorithms, the original version of the SO algorithm starts by generating a random population to begin the optimization process. This process is carried out as represented in (15):

$$X_i = X_{min} + rand(X_{max} - X_{min}), \quad (15)$$

where X_i denotes the position of the i-th individual, *rand* is a random number between 0 and 1, while X_{max} and X_{min} are the upper and lower boundaries of the design variables.

This paper proposes a chaotic version of the SO algorithm, named the chaotic-snake optimization (C-SO) algorithm. The proposed algorithm initializes the population using chaotic Gauss mapping [24] instead of conventional random initialization. The equations that describe the initialization process using chaotic Gauss mapping are given as follows:

$$\begin{aligned} y_1 &= rand, \\ y_{i+1} &= exp(-\alpha y_i{}^2) + \beta, \\ X_i &= X_{min} + y_i(X_{max} - X_{min}). \end{aligned} \quad (16)$$

The parameters α and β are related to the width and height of the Gaussian curve, respectively. Interesting chaotic properties occur around $-1 \le \beta \le 1$ on the Gauss map, where the map's value asymptotically oscillates around −1 and 1.25. The parameters α and β are set to 4.9 and −0.58, according to the original version of Gauss chaotic maps. The main advantage of embedding chaotic maps into the initialization process is obtaining an optimal initial population for the optimization process. Obtaining a good starting population ensures that the proposed chaotic version of the algorithm will converge to the optimal solution faster than the original version.

The iterative process starts with dividing the population into male and female snakes. Assuming an equal number of male and female snakes in the population, if we denote the total number of individuals in the population as N, the number of male snakes as N_m, and the number of female snakes as N_f, the following equations can be applied:

$$\begin{aligned} N_m &\approx N/2, \\ N_f &= N - N_m. \end{aligned} \quad (17)$$

Afterward, the temperature T and food quantity Q must be calculated:

$$\begin{aligned} T &= exp\left(-\frac{ite}{max_{ite}}\right), \\ Q &= c_1\, exp\left(\frac{ite - max_{ite}}{max_{ite}}\right). \end{aligned} \quad (18)$$

where *ite* stands for the current iteration, max_{ite} denotes the maximum number of iterations, and c_1 is a constant that equals 0.5 [23].

If the Q value is less than the selected threshold (0.25 in [23]), the snakes do not have enough food and must search for it. This phase is called the exploration phase, and the positions of male and female snakes are updated according to the following equations:

$$X_{i,m}(ite+1) = X_{rand,m}(ite) \pm c_2 A_m\left((X_{max} - X_{min})rand + X_{min}\right),$$
$$X_{i,f}(ite+1) = X_{rand,f}(ite) \pm c_2 A_f\left((X_{max} - X_{min})rand + X_{min}\right). \quad (19)$$

where $X_{i,m}$ and $X_{i,f}$ denote the positions of the i-th male and female snakes, while $X_{rand,m}$ and $X_{rand,f}$ stand for random male and female snakes, respectively. In the previous equations, A_m and A_f denote the male and female ability to find food and can be calculated as follows:

$$A_m = exp\left(-\frac{f_{rand,m}}{f_{i,m}}\right),$$
$$A_f = exp\left(-\frac{f_{rand,f}}{f_{i,f}}\right). \quad (20)$$

where $f_{rand,m}$ and $f_{rand,f}$ stand for the fitness function values for individuals $X_{rand,m}$ and $X_{rand,f}$. Like this, $f_{i,m}$ and $f_{i,f}$ denote the fitness function values for individuals $X_{i,m}(ite)$ and $X_{i,f}(ite)$.

Otherwise, if Q is higher than the threshold value, the food exists, and the exploitation phase occurs. Furthermore, it is necessary to examine the temperature T. If T is higher than a certain temperature threshold (selected to be 0.6 as in [23]), the weather is hot, and the snakes will move to the food. In that case, the position of the i-th snake $X_{i,j}$ is updated according to the following equation:

$$X_{i,j}(t+1) = X_{food} \pm c_3 T.rand\left(X_{food} - X_{i,j}(t)\right), \quad (21)$$

where c_3 is a constant set to 2 [23], and X_{food} is the position of the best snake, i.e., the snake whose fitness function has the lowest value. On the other hand, if the temperature T is lower than the threshold, the snakes will fight or mate. In the fight mode, the positions of $X_{i,m}$ and $X_{i,f}$ are updated as follows:

$$X_{i,m}(t+1) = X_{i,m}(t) \pm c_3 FM.rand\left(X_{best,f} - X_{i,m}(t)\right),$$
$$X_{i,f}(t+1) = X_{i,f}(t) \pm c_3 FF.rand\left(X_{best,m} - X_{i,f}(t)\right). \quad (22)$$

In the previous equations, $X_{best,f}$ and $X_{best,m}$ are the best snakes selected from the female and male populations, respectively. Additionally, FM and FF denote the fighting ability of male and female snakes:

$$FM = exp\left(-\frac{f_{best,f}}{f_i}\right),$$
$$FF = exp\left(-\frac{f_{best,m}}{f_i}\right). \quad (23)$$

where $f_{best,f}$ and $f_{best,m}$ stand for the fitness function value of the best female and male snakes. Additionally, f_i denotes the fitness function value of the i-th individual.

In the mating mode, the positions of the male and female snakes can be calculated using the following equations:

$$X_{i,m}(t+1) = X_{i,m}(t) \pm c_3 M_m.rand\left(QX_{i,f}(t) - X_{i,m}(t)\right),$$
$$X_{i,f}(t+1) = X_{i,f}(t) \pm c_3 M_f.rand\left(QX_{i,m}(t) - X_{i,f}(t)\right). \quad (24)$$

where M_m and M_f denote the mating abilities of male and female snakes, respectively. Thus:

$$M_m = exp\left(-\frac{f_{i,f}}{f_{i,m}}\right), \quad (25)$$

$$M_f = exp\left(-\frac{f_{i,m}}{f_{i,f}}\right).$$

In the previous equations, $f_{i,f}$ and $f_{i,m}$ are the fitness function values of $X_{i,f}(ite)$ and $X_{i,m}(ite)$. Finally, the last step of the iteration is to select the worst male snake $X_{worst,m}$ and the worst female snake $X_{worst,f}$ and replace them as follows:

$$X_{worst,m} = X_{min} + rand(X_{max} - X_{min}),$$
$$X_{worst,f} = X_{min} + rand(X_{max} - X_{min}). \quad (26)$$

The steps of the proposed C-SO algorithm are summarized in the pseudo-code given in Algorithm 1. Additionally, the flowchart shown in Figure 8 depicts the steps of the C-SO algorithm.

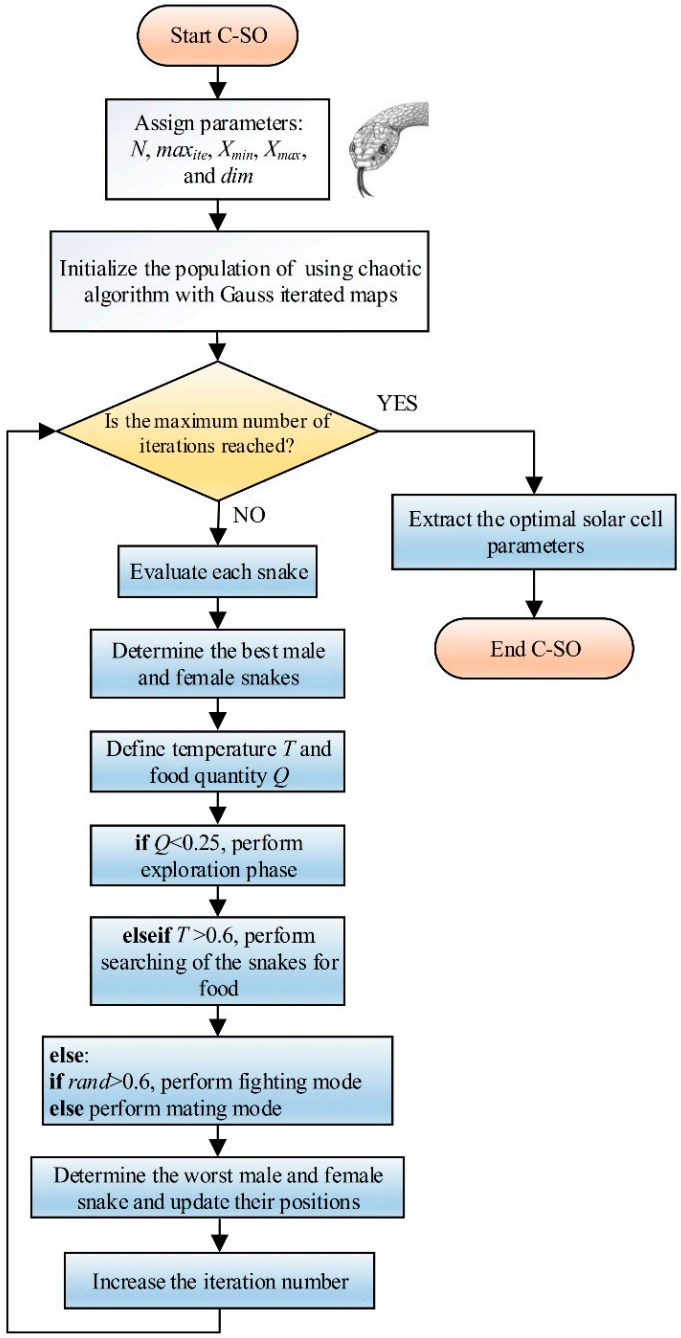

Figure 8. Flowchart of the C-SO algorithm.

Algorithm 1. Procedure of the proposed C-SO algorithm.

1: Set parameters N, max_{ite}, X_{min}, $X_{max,}$ and dimension
2: Initialize the population using Gauss chaotic maps
3: Divide the population N into 2 equal groups–male and female
4: **for** ite = 1 to max_{ite}
5: Evaluate each snake from the male and female group
6: Find the best male $f_{best,m}$ and best female $f_{best,f}$ snake
7: Define temperature T and food quantity Q
8: **if** (Q < 0.25)
9: Perform the exploration phase
10: **else if** (T > 0.6)
11: The snakes will move to the food-exploitation phase
12: **else**
13: **if** ($rand$ > 0.6)
14: Perform the fighting mode of the snakes
15: **else**
16: Perform mating of the snakes
17: Find the worst male and female snake and update them
18: **end if**
19: **end if**
20: **end for**
21: Return the best solution

5. Numerical Results

This section presents the results of applying the C-SO algorithm to estimate the parameters for standard and proposed solar cell models. The estimation process is used for RTC France solar cell and the Photowatt-PWP201 module. The goal of the estimation process was the minimization of the RMSE represented in Equation (5). However, the current for the proposed circuit was calculated using Equations (8), (11), and (14) based on the circuit type. The results are presented in Table 1 for RTC France solar cell and Table 2 for the Photowatt-PWP201 module. Besides, in Tables 1 and 2, the values of RMSE calculated for all SDM circuits are also given.

The current-voltage characteristics, power-voltage characteristics, corresponding current-voltage errors, corresponding power-voltage errors, series resistance–voltage, and parallel resistance–voltage characteristics for both RTC France solar cell and Photowatt-PWP201 module are explored in Figures 9 and 10. Several conclusions can be derived based on the presented results in Tables 1 and 2 and Figures 9 and 10 for both RTC France solar cell and the Photowatt-PWP201 module.

- The proposed algorithm is very efficient in estimating parameters for RTC France solar cell and the Photowatt-PWP201 module, as it enables parameters determination with a lower RMSE value than methods listed in Tables A1 and A2.
- Recalling Section 2, the RMSE for RTC France solar cell determined for standard SDM is $7.730062689943169 \times 10^{-4}$, slightly better than the results available in the literature. For the Photowatt-PWP201 module, the RMSE is 0.002039992273216, which is a better result than the results available in the literature.
- Additionally, the voltage dependence of R_P or R_S or both enables better fitting between the measured and simulated characteristics for both investigated solar cells/modules.
- The impact of voltage dependence on individual series or parallel resistance cannot be generally guaranteed as a better effect of the voltage dependence of series resistance for the Photowatt-PWP201 module on the results was observed in Table 2. In contrast, a better impact of the voltage dependence of the parallel resistance for the RTC France solar cell was observed in Table 1.

- The value of RMSE can be reduced by 40% for the Photowatt-PWP201 module and 20% for RTC France solar cell, considering the voltage dependence of both resistances in the solar cell model. Therefore, the matching between measured and simulated curves is significantly improved.

Table 1. Estimated parameters value for the proposed equivalent circuits for the investigated RTC France solar cell.

Parameter	Standard SDM	SDM$_{RS}$	SDMR$_P$	SDMR$_P$R$_S$
I_{pv} (A)	0.7607879665080	0.7608049248859	0.7610468429411	0.7613631203879
I_0 (μA)	0.3106846042013	0.2991003927335	0.2310892217190	0.0409996462319
n	1.4772677889166	1.4734669046357	1.4488935673420	1.3045585894008
R_S (Ω)	0.0365469451928	-	0.0373848509444	
R_P (Ω)	52.8897883285066	52.6797662689792	-	
R_{S0} (Ω)	-	0.0376221542230	-	0.0618725707814
R_{P0} (Ω)	-		66.7442335923146	83.3942065127408
k_{n-Rs}	-	0.0440721596083	-	0.5094232140590
k_{n-Rp}	-	-	0.8898254600473	1.5685793413223
$RMSE \times 10^{-4}$	7.7300626899432	7.7289464947487	6.9494430170526	6.1899974615364

Table 2. Estimated parameters value for the proposed equivalent circuits for the investigated Photowatt-PWP201 module.

Parameter	Standard SDM	SDM$_{RS}$	SDMR$_P$	SDMR$_P$R$_S$
I_{pv} (A)	1.0323575940489	1.0342899634638	1.0336560526298	1.0385507500932
I_0 (μA)	2.4965956963769	0.5898019648459	3.1895652071363	0.1402290648789
n	47.3985550384409	42.6481872737510	48.2903258581200	38.7679613812771
R_S (Ω)	1.2405473296235	-	1.2205195472483	-
R_P (Ω)	748.323004851098	636.813538190211	-	-
R_{S0} (Ω)	-	2.1086757391782	-	2.8316185090761
R_{P0} (Ω)	-	-	414.225359045698	404.119541040858
k_{n-Rs}	-	0.0211826846962	-	0.0288655047700
k_{n-Rp}	-	-	−0.0848837309056	−0.0270864444391
$RMSE$	0.0020399922732	0.0015210625963	0.0018322922805	0.0012129409135

Finally, to test the proposed algorithm's efficiency over other known algorithms, we compared the original variant of the SO algorithm, the proposed C-SO, particle swarm optimization (PSO), the Aquila optimizer (AO) algorithm and henry gas solubility optimization (HGSO). The results were compared using the same starting conditions and the number of iterations. The algorithm ran 30 independent times, and the best, worst, mean, median, and standard deviation (STD) results were calculated for the same number of iterations. A summary of the results obtained is presented in Table 3.

Additionally, using the collected data, we performed the Wilcoxon *p*-value test, and the results obtained are given in Table 4. Based on these results, it is evident that the C-SO algorithm enables improvement of the original SO algorithm, outperforming the other algorithms. Additionally, based on the Wilcoxon *p*-value test, chaotic sequence improved the repeatability of the results. The convergence curve for the algorithms considered in the Wilcoxon *p*-value test is presented in Figure 11. Based on these results, it is evident that the proposed C-SO algorithm is superior to other literature-known algorithms.

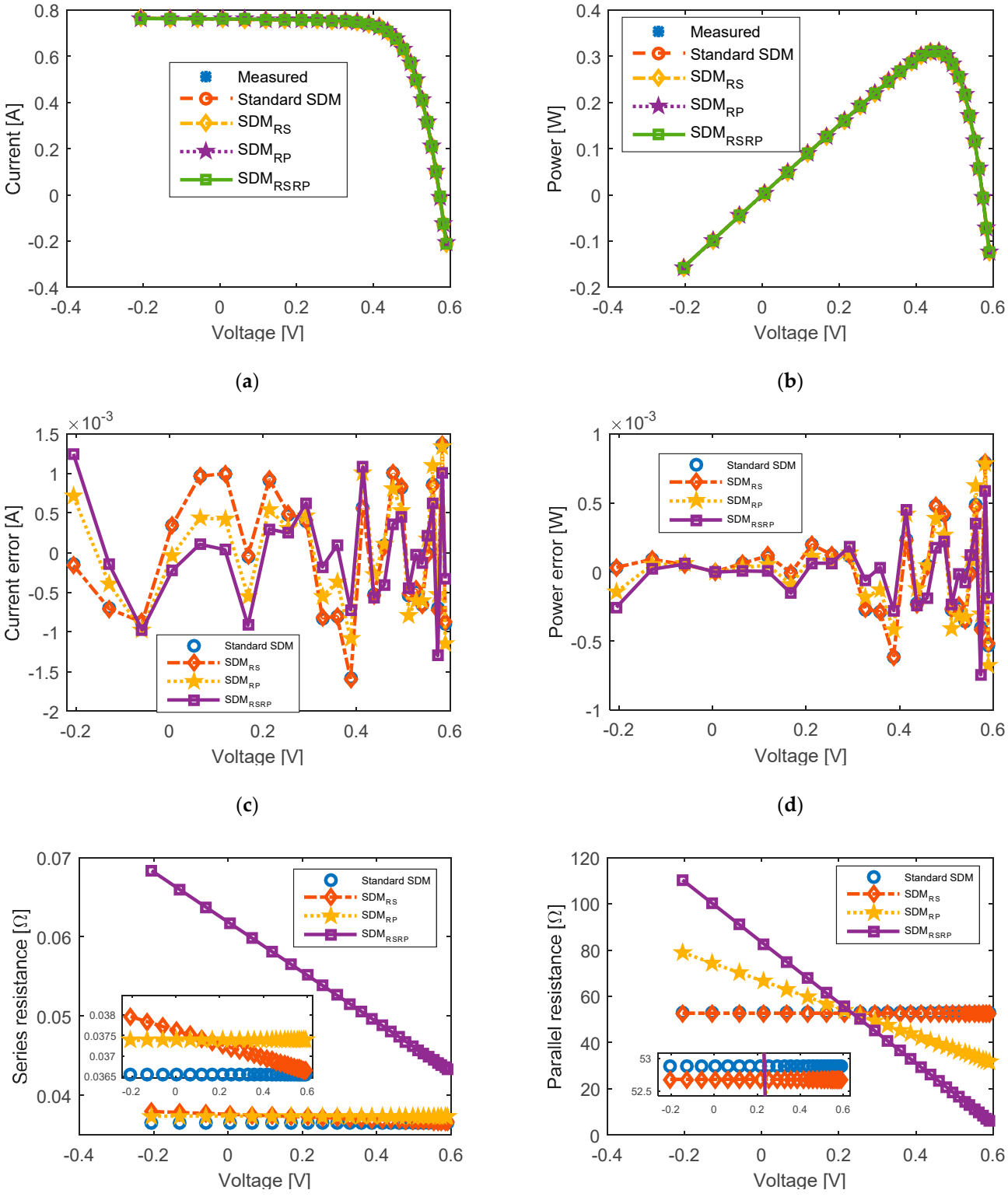

Figure 9. RTC France solar cell: (**a**) current-voltage characteristics; (**b**) power-voltage characteristics; (**c**) corresponding current-voltage errors; (**d**) corresponding power-voltage errors; (**e**) series resistance–voltage dependence characteristics; (**f**) parallel resistance–voltage dependence characteristics.

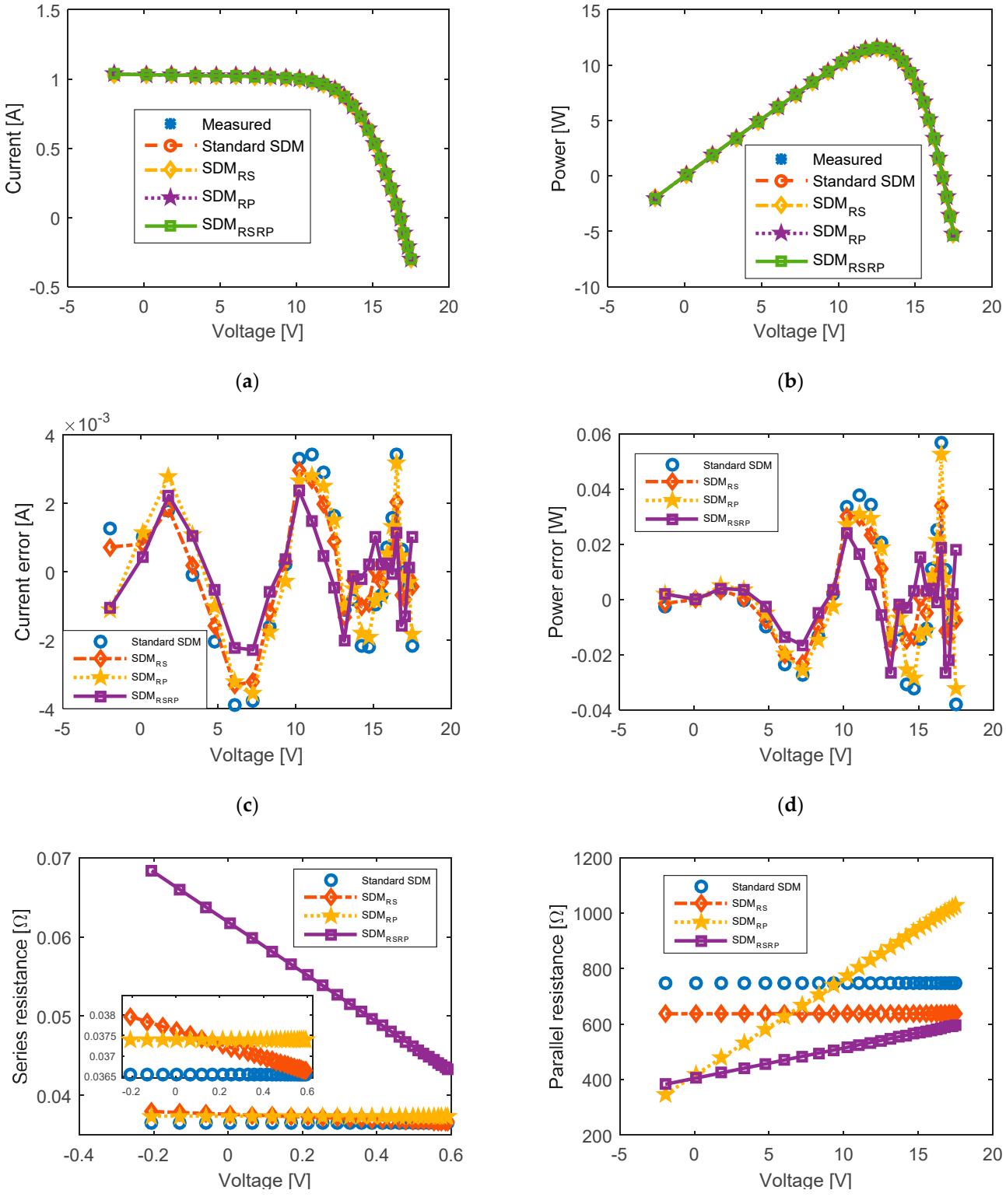

Figure 10. Photowatt-PWP201 module: (**a**) current-voltage characteristics; (**b**) power-voltage characteristics; (**c**) corresponding current-voltage errors; (**d**) corresponding power-voltage errors; (**e**) series resistance–voltage dependence characteristics; (**f**) parallel resistance–voltage dependence characteristics.

Table 3. Statistical measures for the obtained results using different algorithms over 30 independent runs.

Measure	C-SO Proposed	Original SO	PSO	AO	HGSO
Best	$7.730066720825 \times 10^{-4}$	$7.730112887551 \times 10^{-4}$	$7.757602348738 \times 10^{-4}$	0.00288037656117	0.00526106472624
Worst	$8.468025234636 \times 10^{-4}$	$8.322080126651 \times 10^{-4}$	0.00198685445976	0.00851885985240	0.01474037311829
Mean	$7.826453665352 \times 10^{-4}$	$7.831299232730 \times 10^{-4}$	0.00105448589746	0.00556610811629	0.01091282953358
Median	$7.784837234895 \times 10^{-4}$	$7.786564960706 \times 10^{-4}$	$9.853004240075 \times 10^{-4}$	0.00574743127044	0.01118504603992
Std	$1.408324862610 \times 10^{-5}$	$1.234187862853 \times 10^{-5}$	$3.249036540248 \times 10^{-4}$	0.00145918070830	0.00250149664426

Table 4. Wilcoxon test results.

C-SO versus SO	C-SO versus AO	C-SO versus HGSO	C-SO versus PSO
$6.84322586762450 \times 10^{-3}$	$3.019859359162151 \times 10^{-11}$	$3.019859359162151 \times 10^{-11}$	$1.856733730733403 \times 10^{-9}$

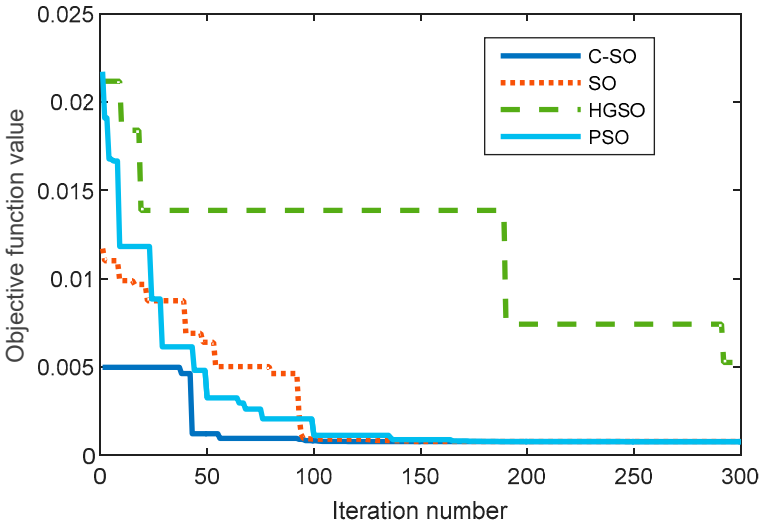

Figure 11. Convergence curve of C-SO versus different algorithms.

6. Experimental Verification

The usefulness of using the new equivalent schemes and the new algorithm to estimate solar cell parameters was covered in the previous section. The applicability of the modified models to a solar laboratory module (part of the laboratory set Clean Energy Trainer) is examined in this section. The method of measurement is as follows. Connect the PC device first, then the USB data monitor, solar cells, and then the USB data monitor. A PC and an active component, such as a solar cell, are connected via a power-electronic device called a USB data monitor. This tool makes it possible to test voltages and currents and scales the results on the computer. Solar cells must also be connected in parallel or in series. After that, we measured the solar module's temperature, activated solar measurement equipment (in our case, the TES 133R), and set solar lamps at a specific distance. It is required to specify the current and measure the voltage values using the Clean Energy Trainer program loaded on the PC, checking the temperature and insolation of the solar cell or module during all measurements. Figure 12 shows a block diagram of all devices connected.

Measurements were carefully performed, monitoring all variables (irradiance—1335 W/m^2, temperature 44 °C, voltage and current measures). The obtained results are then used for solar cell parameters estimation. Furthermore, we determined solar cell parameters for all equivalent circuits proposed. The results are summarized in Table 5. The measured and estimated characteristics of current, power, current error, power error, series resistance-voltage, and parallel resistance-voltage versus voltage are depicted in Figure 13.

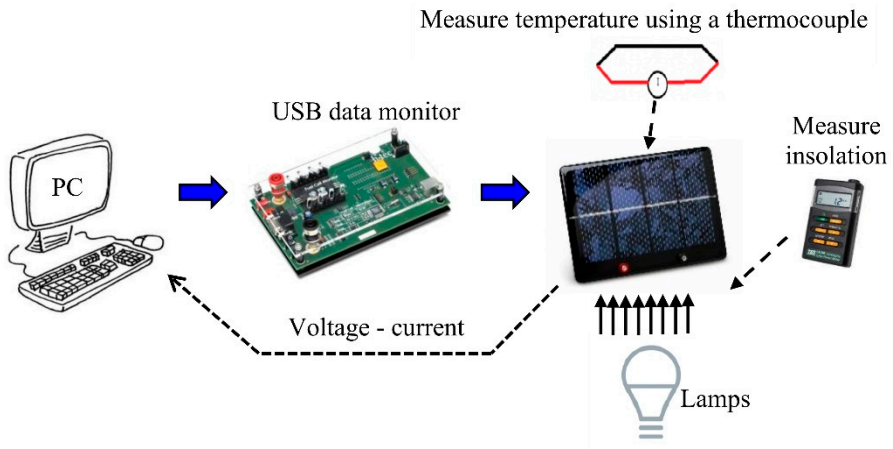

Figure 12. Experimental setup of the solar laboratory module.

Table 5. Estimated parameters value for proposed equivalent circuits for the observed solar laboratory module.

Parameter	Standard SDM	SDM_{RS}	$SDMR_P$	$SDMR_PR_S$
I_{pv} (A)	0.573103853383459	0.574513627819549	0.573197838345865	0.573000469924812
I_0 (μA)	0.306664697651680	0.303792633051805	0.303290021746827	0.302816131087847
n	0.388241333333333	0.388215384615385	0.388215384615385	0.388214999538461
R_S (Ω)	0.058300000000000	-	0.0570	-
R_P (Ω)	120.79060	116.907	-	-
R_{S0} (Ω)	-	0.0581	-	0.057
R_{P0} (Ω)	-	-	117.227264	116.8833792
k_{n-Rs}	-	−0.0111	-	− 0.0125
k_{n-Rp}	-	-	0.013110	0.023110
RMSE	0.001940250703697	0.001605316586546	0.001583230030742	0.001504856980387

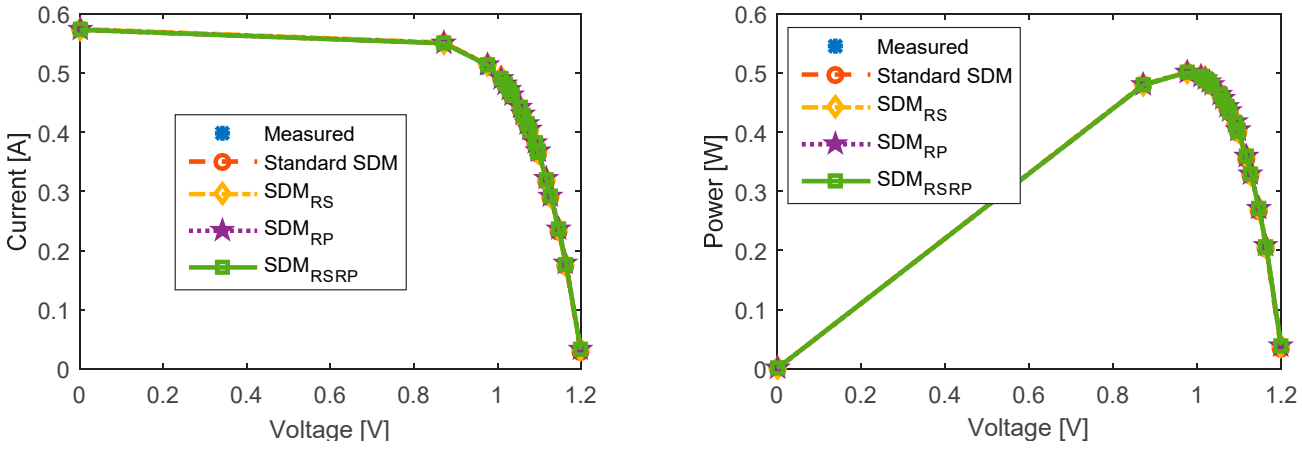

(**a**) (**b**)

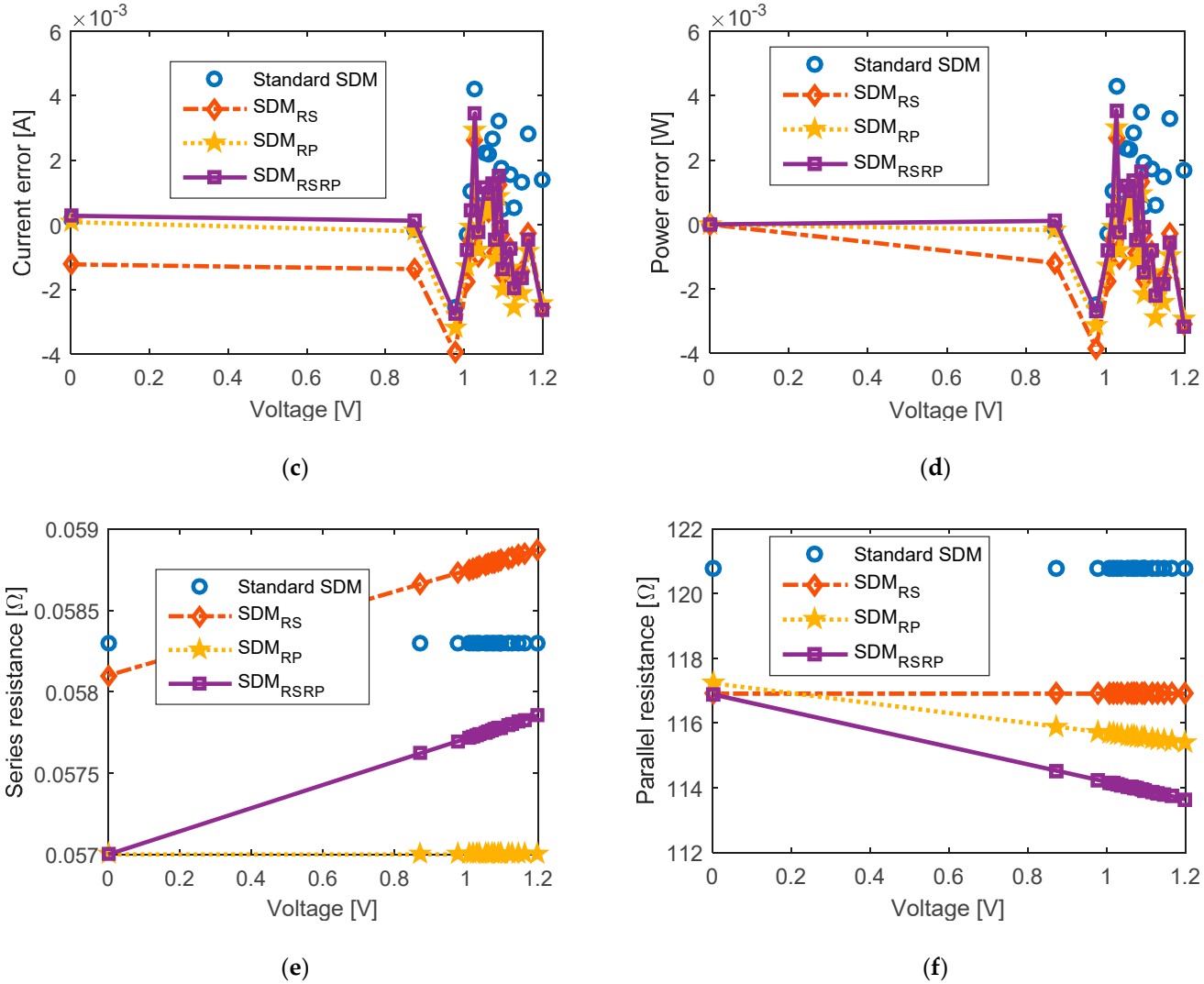

Figure 13. Solar laboratory module: (**a**) current-voltage characteristics; (**b**) power-voltage characteristics; (**c**) corresponding current-voltage errors; (**d**) corresponding power-voltage errors; (**e**) series resistance–voltage dependence characteristics; (**f**) parallel resistance–voltage dependence characteristics.

The first conclusion from all the results presented is that the results are close to each other (as evident in Figure 13 and current and voltage errors in Table 5). Second, the agreement between measured and estimated characteristics is remarkable for all figures. Third, the lowest value of RMSE gives the usage of the equivalent circuit with both resistance variables as a function of voltage. Therefore, for this example it is evident that the proposed equivalent circuits are effective for the current-voltage representation of solar cells. Additionally, the proposed algorithm enables effective solar cell parameter determination.

7. Conclusions

The selection of an appropriate equivalent circuit and the calculation of its parameters are necessary for modeling PV solar cells. In this regard, three new PV equivalent circuits are proposed in this study, in contrast to the many methods proposed in the literature, typically based on basic PV equivalent circuits and modified versions with added resistance. The definition of appropriate resistance as a voltage function gives the proposed schemes their originality.

The analytical equations for all three equivalent circuits are included in the study. The Lambert W function was used to express the current-voltage dependence solution. The C-SO algorithm for determining the solar cell equivalent circuit's parameters was also put forth in this work.

The RTC France solar cell and the Photowatt-PWP201 module's parameter estimates were carried out utilizing the proposed algorithm and the proposed equivalent circuits. The findings demonstrated that using the suggested methods, as opposed to conventional equivalent circuits, significantly reduces the RMSE between the measured and estimated values. Additionally, the error can be decreased by up to 20% with RTC France and up to 40% with the Photowatt-PWP201 module. The Clean Energy Trainer setup laboratory cell underwent the same analysis.

Future works will consider the voltage-dependent resistance of double and triple solar cell models for careful investigation of the mathematical analysis of these equivalent solar cell circuit designs. Additionally, new techniques for estimating the characteristics of solar cells will be developed with a specific focus on new hybrid optimization techniques.

Author Contributions: Conceptualization, M.C., M.V., S.H.E.A.A.; methodology, M.R., M.C., M.M.; validation, S.A., A.A.A., A.S.A., M.C.; formal analysis, M.C., S.H.E.A.A.; investigation, M.V., M.R.; resources, M.C., M.M., Z.M.A.; data curation, M.C., S.H.E.A.A.; writing—original draft preparation, M.C.M.V., M.R.; writing—review and editing, S.A., A.A.A., A.S.A., S.H.E.A.A.; visualization, M.M., M.C., and S.H.E.A.A. All authors have read and agreed to the published version of the manuscript.

Funding: The Deanship of Scientific Research (DSR) at King Abdulaziz University, Jeddah, Saudi Arabia, funded this project under grant no. (RG-19-135-43).

Data Availability Statement: Not applicable.

Acknowledgments: The authors acknowledge the Deanship of Scientific Research (DSR) at King Abdulaziz University, Jeddah, Saudi Arabia, for funding this project under grant no. (RG-19-135-43). The Authors also acknowledge the support provided by King Abdullah City for Atomic and Renewable Energy (K.A.CARE) under K.A.CARE-King Abdulaziz University Collaboration Program.

Conflicts of Interest: The authors declare no conflict of interest.

Abbreviations

ABC	Artificial bee colony
ABCTRR	Trust-region reflective (TRR) deterministic algorithm with the artificial bee colony (ABC) metaheuristic algorithm
ABSO	General algorithm for finding the absolute minimum of a function to a given accuracy
AGDE	Adaptive guided differential evolution
ALO	Ant Lion optimization algorithm
BBO	Biogeography-based optimization
BPFPA	Bee pollinator flower pollination algorithm
BLPSO	Biogeography-based learning particle swarm optimization
BLPSO	Biogeography-based learning PSO
BHCS	Hybridizes cuckoo search (CS) and biogeography-based
BMO	Bird mating optimization
BSA	Backtracking search algorithm
CPSO	Chaos particle swarm optimization
CS	Cuckoo search
CSO	Competitive swarm optimizer
CSA	Competitive swarm algorithm
CMM-DE/BBO	DE/BBO with covariance matrix-based migration
CLPSO	Comprehensive learning particle swarm optimization
CIABC	Chaotic improved the artificial bee colony

CNSMA	Boosting slime mould algorithm
COA	Chaotic optimization approach
COOA	Coyote optimization algorithm
CWOA	Chaotic whale optimization algorithm
CPSO	Conventional PSO
CPMPSO	Classified perturbation mutation-based PSO
DGM	Dynamic gaussian mutation
DE	Differential evolution
DE/BBO	Hybrid differential evolution with biogeography-based optimization
DE/WOA	Differential evolution/whale optimization algorithm
EHHO	Enhanced Harris Hawks optimization
ERWCA	Evaporation rate water cycle algorithm
EDDM-LW	Explicit double-diode model based on the Lambert W function
EO	Equilibrium optimizer
EOTLBO	Equilibrium optimizer teaching-learning-based optimization
EJADE	Enhanced joint approximation diagonalization of Eigen matrices algorithm
ELPSO	Enhanced leader particle swarm optimization
ELBA	Efficient layer-based routing algorithm
EGBO	Enhanced gradient-based optimization
EVPS	Enhanced vibrating particles systems
FA	Firefly algorithm
FCEPSO	Fractional chaotic ensemble particle swarm optimizer
FPA	Flower pollination algorithm
FPSO	Fuzzy particle swarm optimization
HCLPSO	Chaotic heterogeneous comprehensive learning particle swarm optimizer variants
HPSOSA	Hybrid particle swarm optimization and simulated annealing
HFAPS	Hybrid firefly and pattern search algorithms
HISA	Hyperplanes intersection simulated annealing
HS	Harmony search
HSMAWOA	Hybrid novel slime mould algorithm with a whale optimization algorithm
GA	Genetic algorithm
GABC	Gbest guided ABC
GAMNU	Genetic algorithm based on non-uniform mutation
GAMS	General algebraic modeling system
GCPSO	Guaranteed convergence particle swarm optimization
GGHS	Gaussian global-best harmony search
GSK	Gaining-sharing knowledge-based algorithm
GOTLBO	Generalized oppositional teaching learning-based optimization
GOFPNAM	Algorithm based on FPA, the Nelder-Mead simplex, and the GOBL mechanism
GBABC	Gaussian bare-bones ABC
GWO	Grey wolf optimizer
GWOCS	Grey wolf optimizer cuckoo search
HS	Harmony search
HHO	Harris Hawks optimization
HCLPSO	Heterogeneous comprehensive learning particle swarm optimizer
ICA	Independent component analysis
ISCA	Improved sine cosine algorithm
ISCE	Improved shuffled complex evolution
ISMA	Index-based subgraph matching algorithm
IADE	Improved differential evolution algorithm
IBBGOA	Interval branch and bound global optimization algorithm
IJAYA	Improved JAYA
IGHS	Improved Gaussian harmony search
IMFO	Improved moth-flame optimization
ITLBO	Improved teaching-learning-based optimization
IWOA	Improved whale optimization algorithm
JADE	Joint approximation diagonalization of Eigen matrices algorithm

jDE	Self-adaptive DE algorithm
LAPO	Lightning attachment procedure optimization
LCJAYA	Logistic chaotic JAYA algorithm
LETLBO	TLBO with a learning experience of other learners
LBSA	List-based simulated annealing algorithm
LSP	Loop of the search process
LMSA	Least mean squares (LMS) algorithms
MADE	Memetic adaptive differential evolution
MABC	Modified ABC
MJA	Modified JAYA algorithm
MLBSA	Modified list-based simulated annealing algorithm
MPA	Marine predator algorithm
MFO	Moth-flame Optimization
MPSO	Particle swarm optimization with adaptive mutation strategy
MPCOA	Mutative-scale parallel chaos optimization algorithm
MRFO	Manta ray foraging optimization
MSSO	Modified simplified swarm optimization
MVO	Multi-verse optimizer
nm-NMPSO	Nelder-Mead and modified particle swarm optimization
NMMFO	Nelder–Mead moth flame method
NIWTLBO	Non-linear inertia weighted TLBO
NRM	Newton Raphson method
NPSOPC	Niche particle swarm optimization in parallel computing
ODE	Opposition-based differential evolution
PGJAYA	Performance-guided JAYA
pSFS	Perturbed stochastic fractal search
PS	Pattern search
PSO	Particle swarm algorithm
PPSO	Parallel particle swarm optimization
RLDE	Run length encoding (RLE) compression algorithm
RTLBO	Ranking teaching-learning-based optimization
R-II	Rao-2 algorithm
R-III	Rao-3 algorithm
SA	Simulated annealing
SaDE	Self-adaptive differential evolution algorithm
SDA	Successive discretization algorithm
SDE	Stochastic differential evolution
SGDE	Stochastic gradient descent algorithm
SHADE	Success-history-based parameter adaptation for differential evolution
SCA	Sine cosine algorithm
SATLBO	Self-adaptive teaching-learning-based optimization
SMA	Slime mould algorithm
SFS	Stochastic fractal search
STLBO	Simplified TLBO
SATLBO	Simulated annealing TLBO
SOS	Symbiotic organisms search
SSA	Salp swarm algorithm
SSO	Simplified swarm optimization
TLABC	Teaching-learning-based artificial bee colony
TLBO	Teaching-learning-based optimization
TLO	Teaching-learning optimization
TVACPSO	Time-varying acceleration coefficients particle swarm optimization
TVAPSO	Time-varying particle swarm optimization
WLCSODGM	Winner-leading CSO with DGM
WCMFO	Hybrid algorithm based on the water cycle and moth-flame optimization algorithm
WOA	Whale optimization algorithm
WDO	Wind-driven optimization

WHHO Whippy harris hawks optimization

Appendix A

Table A1. Parameters values of the RTC France solar cell.

Method	Reference	Algorithm	I_{pv} (A)	I_0 (μA)	n	R_S (Ω)	R_P (Ω)
1	[15]	EO	0.760759704	0.32628893	1.482193	0.036341	54.206594
2		MPA	0.76079	0.31072	1.4771	0.036546	52.8871
3		HCLPSO	0.76079	0.31062	1.4771	0.036548	52.885
4		BPFPA	0.76	0.3106	1.4774	0.0366	57.7151
5		ER-WCA	0.760776	0.322699	1.48108	0.036381	53.691
6		MPSO	0.760787	0.310683	1.475262	0.036546	52.88971
7		PS	0.7617	0.998	1.6	0.0313	64.10236
8	[25]	BBO-M	0.7607	3.19×10^{-1}	1.4798	0.03642	53.36227
9		IMFO	0.7607	3.23×10^{-1}	1.4812	0.03638	53.71456
10		MFO	0.7609	3.01×10^{-1}	1.4694	0.03596	52
11		WCMFO	0.7607	3.23×10^{-1}	1.4812	0.03638	53.69502
12		SCA	0.765	6.79×10^{-1}	1.5609	0.03544	50.14796
13		CSO	0.7608	3.23×10^{-1}	1.4812	0.03638	53.7185
14		SA	0.762	4.80×10^{-1}	1.5172	0.0345	43.103
15	[12]	WHHO	0.76077551	0.32302031	1.48110808	0.0363771	53.71867407
16		EHHO	0.760775	0.323	1.481238	0.036375	53.74282
17		PGJAYA	0.7608	0.323	1.4812	0.0364	53.7185
18		FPSO	0.7607	0.323	1.4811	0.03637	53.7185
19		IJAYA	0.7608	0.3228	1.4811	0.0364	53.7595
20		BMO	0.7607	0.3247	1.4817	0.0363	53.8716
21		GOTLBO	0.7608	0.3297	1.4833	0.0363	53.3664
22		ABSO	0.7608	0.30623	1.47583	0.03659	52.2903
23		PSO	0.7607	0.4	1.5033	0.0354	59.012
24		GA	0.7619	0.8087	1.5751	0.0299	42.3729
25		GAMNU	0.760774	0.3255954	1.482096	0.0363402	53.89686
26		Rcr-IJADE	0.760776	0.323021	1.481187	0.036377	53.718526
27		DE/BBO	0.7605	0.3248	1.48149	0.0364	53.8753
28		BBO-M	0.76078	0.3187	1.47984	0.03642	53.36227
29		TLBO	0.7607	0.3294	1.4831	0.0363	54.3015
30		MFO	0.760796	0.3086	1.476593	0.0365579	52.50655869
31		JAYA	0.7608	0.3281	1.4828	0.0364	54.9298
32		IADE	0.7607	0.33613	1.4852	0.03621	54.7643
33	[26]	CSA	0.768929	0.318	1.479628	0.0364559	52.44667219
34		ABSO	0.7608	0.30623	1.47878	0.03659	52.2903
35		LBSA	0.7609	0.32583	1.482	0.0364	54.1083
36		HS	0.7607	0.30495	1.47538	0.03663	53.5946
37		CLPSO	0.7608	0.34302	1.4873	0.0361	54.1965
38		ABC	0.7609	0.33243	1.4842	0.0363	55.461
39		HHO	0.759864	0.39375	1.5012327	0.035536	76.1719
40		CPSO	0.7607	0.4	1.5033	0.0354	59.012
41		GWO	0.769969	0.91215	1.596658	0.02928	18.103
42		CNMSMA	0.760776	0.323017	1.481182	0.036377	53.71821
43		IJAYA	0.760782	0.29953	1.474962	0.036685	51.33013
44	[27]	GOTLBO	0.760784	0.303556	1.474962	0.036645	52.38834
45		MLBSA	0.760777	0.323118	1.481214	0.036376	53.70918
46		GOFPANM	0.760776	0.323021	1.481184	0.036377	53.71853
47		SMA	0.76076	0.32314	1.48114	0.03637	53.71489
48	[17]	Rao	0.76102	0.32312	1.48122	0.03642	53.74568
49		TLO	0.76088	0.33288	1.48466	0.03542	56.03045
50		ABC	0.76054	0.35999	1.49595	0.03602	52.14795

51		PSO	0.76082	0.33018	1.48334	0.03624	53.59878
52		CS	0.76078	0.32954	1.48305	0.03644	54.30202
53		BMO	0.76077	0.32479	1.48173	0.03636	53.8716
54		CPSO	0.7607	0.4	1.5033	0.0354	59.012
55	[4]	HS	0.7607	0.30495	1.47538	0.03663	53.5946
56		GGHS	0.76092	0.3262	1.48217	0.03631	53.0647
57		IGHS	0.76077	0.34351	1.4874	0.03613	53.2845
58		ABSO	0.7608	0.30623	1.47583	0.03659	52.2903
59		AGDE	0.76077553	0.32301967	1.48118324	0.0363771	53.7183869
60		DE/WOA	0.76077553	0.32302081	1.48118359	0.0363771	53.7185247
61		PPSO	0.76077567	0.32310012	1.48120841	0.0363761	53.72033352
62		IJAYA	0.76072096	0.33004162	1.48335168	0.0362947	54.79216937
63		TLBO	0.76091513	0.32580092	1.48208555	0.0362621	52.16660204
64	[28]	GOTLBO	0.76080276	0.32452976	1.48167104	0.0363235	53.31216674
65		ITLBO	0.76077553	0.32302083	1.4811836	0.0363771	53.71852696
66		RTLBO	0.76078148	0.32693782	1.48240012	0.0363231	53.93402232
67		SATLBO	0.76078638	0.3173289	1.47939597	0.0364469	53.22833431
68		TLABC	0.76077562	0.32238031	1.48098405	0.036385	53.64456083
69		EOTLBO	0.76077553	0.32302083	1.48118359	0.0363771	53.71852514
70		GAMS	0.7607760	0.3230200	1.4811840	0.0363770	53.7185240
71		FPA	0.76079	0.310677	1.47707	0.0365466	52.8771
72		TVA-PSO	0.760788	0.306827	1.475258	0.036547	52.889644
73		BPFPA	0.76	0.3106	1.4774	0.0366	57.7151
74		MPSO	0.760787	0.310683	1.475262	0.036546	52.88971
75		HISA	0.7607078	0.31068459	1.47726778	0.0365469	52.88979426
76		HCLPSO	0.76079	0.31062	1.4771	0.036548	52.885
77	[29]	Rcr-IJADE	0.760776	0.323021	1.481184	0.036377	53.718526
78		CSO	0.76078	0.323	1.48118	0.03638	53.7185
79		ISCE	0.76077553	0.32302083	1.4811836	0.0363771	53.71852771
80		GOFP-ANM	0.7607755	0.3230208	1.4811836	0.0363771	53.7185203
81		IJAYA	0.7608	0.3228	1.4811	0.0364	54
82		SATLBO	0.7608	0.32315	1.48123	0.03638	53.7256
83		IWAO	0.760877519	0.3232	1.48122913	0.0363753	53.73168644
84		ITLBO	0.7608	0.323	1.4812	0.0364	53.7185
85		CPSO	0.760788	0.3106975	1.475262	0.036547	52.892521
86		MPCOA	0.76073	0.32655	1.48168	0.03635	54.6328
87	[30]	TVACPSO	0.760788	0.3106827	1.475258	0.036547	52.889644
88		FPA	0.76079	0.310677	1.47707	0.0365466	52.8771
89		GOFPANM	0.7607755	0.3230208	1.4811836	0.0363771	53.7185203
90		MPSO	0.760787	0.310683	1.475262	0.036546	52.88971
91		Rcr-IJAD	0.760776	0.323021	1.481184	0.036377	53.718526
92		CSO	0.76078	0.323	1.48118	0.03638	53.7185
93		GOTLBO	0.76078	0.331552	1.48382	0.036265	54.115426
94		EHA-NMS	0.760776	0.323021	1.481184	0.036377	53.718521
95		NM-MPSO	0.76078	0.32315	1.48123	0.03638	53.7222
96	[31]	SATLBO	0.7608	0.32315	1.48123	0.03638	53.7256
97		CWOA	0.76077	0.3239	1.4812	0.03636	53.7987
98		IJAYA	0.7608	0.3228	1.4811	0.0364	53.7595
99		GOFPANM	0.7607755	0.3230208	1.4811836	0.0363771	53.7185203
100		R-WCA	0.760776	0.322699	1.48108	0.036381	53.691
101		ABC-TRR	0.760776	0.323021	1.481184	0.036377	53.718521
102		ABC-TRR (key points)	0.761127	0.311818	1.47741	0.036661	53.516288
103		HFAPS	0.760777	0.322622	1.48106	0.0363819	53.6784
104		SA	0.762	0.4798	1.5172	0.0345	43.1034
105	[32]	LSP	0.761	0.3635	1.4935	0.0366	62.574
106		PS	0.7617	0.998	1.6	0.0313	64.1026
107		NRM	0.7608	0.3223	1.4837	0.0364	53.7634

108		HPSOSA	0.7608	0.3107	1.4753	0.0365	52.8898
109		CPSO	0.7607	0.4	1.5033	0.0354	59.012
110		QPSO	0.7606	0.273	1.46	0.037	51.18
111		CM	0.7608	0.4039	1.5039	0.0364	49.505
112		BPFPA	0.76	0.3106	1.4774	0.0366	57.7151
113		HS	0.760700	0.304950	1.475380	0.036630	53.594600
114		IGHS	0.76077	0.34351	1.4874	0.03613	53.2845
115		ABSO	0.7608	0.30623	1.47583	0.03659	52.2903
116		GGHS	0.76092	0.3262	1.48217	0.03631	53.0647
117		GOTLBO	0.76078	0.331552	1.48382	0.036265	54.115426
118		SSO	0.760803	0.321044	1.480468	0.036392	53.152466
119		ABC	0.7608	0.3251	1.4817	0.0364	53.6433
120		BMO	0.76077	0.32479	1.48173	0.03636	53.87
121		MSSO	0.760777	0.323564	1.481244	0.03637	53.742465
122		FA	0.760872	0.258459	1.45907	0.037247	48.3069
123		ITLBO	0.76077553	0.323	1.48118359	0.0363771	53.7185236
124		TLBO	0.76103591	0.298	1.47314963	0.036594	47.7862925
125		MLBSA	0.76077553	0.3230	1.4811835	0.0363771	53.7185461
126	[11]	MADE	0.76078	0.32300	1.48118	0.03638	53.71853
127		CPMPSO	0.76077553	0.323	1.48118309	0.0363771	53.7183835
128		WOA	0.76012199	0.404	1.50384555	0.0356717	70.1196706
129		MTLBO	0.76077553	0.323	1.48118359	0.0363771	53.7185251
130		ELPSO	0.760788	3.11×10^{-1}	1.475256	0.036547	52.889336
131	[33]	CPSO	0.760788	3.11×10^{-1}	1.475262	0.036547	52.892521
132		BSA	0.761051	4.79×10^{-1}	1.519642	0.034695	79.569251
133		ABC	0.761012	3.35×10^{-1}	1.483057	0.035994	48.784551
134		SDA	0.76077300	0.32444600	1.4816400	0.036360	53.842700
135		BHCS	0.76078000	0.32302000	1.481180	0.036380	53.718520
136		HISA	0.76078800	0.31068500	1.4772700	0.036547	52.889790
137		ICSA	0.76077600	0.32302100	1.4817180	0.036377	53.718524
138		CIABC	0.76077600	0.32302000	1.4810200	0.036377	53.718670
139		LAPO	0.76071000	0.96105000	1.5980000	0.031142	99.144000
140		ISCE	0.76077600	0.32302100	1.4811840	0.036377	53.718530
141	[14]	ITLBO	0.76080000	0.32300000	1.481200	0.036400	53.718500
142		SSA	0.76116000	0.89870000	1.590000	0.031595	96.935000
143		SDO	0.76080000	0.32300000	1.48120	0.036400	53.718500
144		GCPSO	0.76080000	0.31068000	1.4773000	0.036550	52.889800
145		pSFS	0.76080000	0.32300000	1.4812000	0.036400	53.718500
146		IBBGOA	0.76077100	0.32345900	1.4820460	0.036373	53.798171
147		ISCA	0.76077600	0.32301700	1.4811820	0.036377	53.718217
148		NMMFO	0.76077600	0.32302100	1.4811840	0.036377	53.718531
149		LFBSA	0.76077600	0.32302100	1.4811840	0.036377	53.718520
150		SGDE	0.76078	0.32302	1.48118	0.03638	53.71853
151		ELBA	0.76078	0.32302	1.48119	0.03638	53.71852
152		EHHO	0.76078	0.323	1.48124	0.03638	53.74282
153	[10]	LCJAYA	0.7608	0.323	1.4819	0.0364	53.7185
154		NPSOPC	0.7608	0.3325	1.4814	0.03639	53.7583
155		GWOCS	0.76077	0.32192	1.4808	0.03639	53.632
156		FC-EPSO	0.76079	0.31131	1.4773	0.03654	52.944
157		WDO	0.7608	0.3223	1.4808	0.036768	57.74614
158		BPFPA	0.76	0.3106	1.4774	0.03666	57.7156
159	[34]	GOTLBO	0.76078	0.3315	1.48382	0.036265	54.115426
160		FPA	0.76079	0.3106	1.47707	0.0365466	52.8771
161		ABSO	0.7608	0.3062	1.47583	0.03659	52.2903
162		HS	0.7607	0.30495	1.47538	0.03663	53.5946
163	[35]	GSK	0.7608	0.3231	1.4812	0.0364	53.7227
164		ABC	0.7606	0.3174	1.479	0.0365	57.0609

165		BBO	0.7608	0.2839	1.4681	0.0373	51.7597
166		DE	0.7608	0.3231	1.4812	0.0364	53.7185
167		JAYA	0.7608	0.3152	1.477	0.0367	55.3139
168		PSO	0.7608	0.3412	1.4868	0.0362	55.0458
169		WOA	0.7608	0.3241	1.4843	0.0358	55.3054
170		TLBO	0.7608	0.3325	1.4839	0.0363	55.3129
171		GOTLBO	0.7608	0.342	1.487	0.0362	53.8599
172		ITLBO	0.7608	0.323	1.4812	0.0364	53.7187
173		RTLBO	0.7608	0.3423	1.4871	0.0361	55.3065
174		SATLBO	0.7608	0.3423	1.487	0.0361	55.3462
175		LETLBO	0.7608	0.3322	1.4809	0.0364	53.6655
176		BSA	0.7608	0.3257	1.4865	0.0363	54.3242
177		TLABC	0.7608	0.3231	1.4812	0.0364	53.7164
178		IWOA	0.7608	0.3232	1.4812	0.0364	53.7185
179		IJAYA	0.7608	0.3228	1.4811	0.0364	53.7959
180		GWO	0.7606	0.22496	1.4455	0.0385	54.6069
181		MVO	0.763	0.39989	1.5027	0.0377	56.3258
182	[16]	SCA	0.7515	0.25606	1.4593	0.0372	54.2298
183		MFO	0.7607	0.39953	1.5029	0.0355	60
184		ALO	0.7601	0.24432	1.4534	0.0375	57.2379
185		MRFO	0.7608	0.30908	1.4767	0.0366	52.7129
186		BPFPA	0.76	0.3106	1.4774	0.0366	57.7151
187	[36]	FPA	0.76077	0.310677	1.47707	0.03654	52.8771
188		ABSO	0.7608	0.30623	1.47583	0.03659	52.2903
189		CPSO	0.7607	0.4	1.5033	0.0354	59.012
190		FPA	0.76079	0.310677	1.47707	0.0365466	52.8771
191		LMSA	0.76078	0.31849	1.47976	0.03643	53.32644
192	[37]	MPCOA	0.76073	0.32655	1.48168	0.03635	54.6328
193		CS	0.7608	0.323	1.4812	0.0364	53.7185
194		ABSO	0.7608	0.30623	1.47583	0.03659	52.2903
195		ABC	0.7608	0.3251	1.4817	0.0364	53.6433
196		CLPSO	0.76064	0.33454	1.48469	0.03623	56.0342
197		BLPSO	0.76063	0.42518	1.5094	0.03523	62.58528
198		ABC	0.76085	0.33016	1.48339	0.03629	53.59884
199	[18]	GOTLBO	0.76077	0.32256	1.48106	0.03637	53.33877
200		TLABC	0.76078	0.32302	1.48118	0.03638	53.71636
201		IJAYA	0.76078	0.32304	1.48119	0.03638	53.71441
202		SFS	0.76078	0.32302	1.48118	0.03638	53.71852
203		pSFS	0.76078	0.32302	1.48118	0.03638	53.71852
204		GAMS	0.760788	0.310684	1.477268	0.036547	52.889789
205		MADE	0.760787	0.310684	1.475258	0.036546	52.889734
206		ITLBO	0.760787	0.310684	1.475258	0.036546	52.88979
207		IMFO	0.760787	0.31083	1.475305	0.036544	52.904381
208	[13]	MLBSA	0.760787	0.310684	1.475258	0.036546	52.88979
209		TVACPSO	0.760788	0.310684	1.475258	0.036546	52.890001
210		IJAYA	0.760822	0.305965	1.473717	0.036634	52.920663
211		CAO	0.760787	0.310684	1.475258	0.036546	52.889778
212		SOS	0.760786	0.310641	1.475244	0.036548	52.905131
213		EVPS	0.76078	0.317061	1.477295	0.036458	53.337698
214		ISMA	0.760775	0.323034	1.481188	0.036377	53.7198
215		IJAYA	0.76076	0.32258	1.481048	0.036378	53.6319
216		GOTLBO	0.760794	0.326744	1.482346	0.036323	53.7571
217	[38]	MLBSA	0.760776	0.323021	1.481184	0.036377	53.7185
218		GOFPANM	0.760776	0.323021	1.481184	0.036377	53.7185
219		EHHO	0.761366	0.475432	1.521366	0.034608	53.655
220		HSMA_WOA	0.762746	0.306559	1.476448	0.0359219	35.3161
221	[39]	TVACPSO	0.760788	0.3106827	1.475258	0.036547	52.889644

222		CPSO	0.760788	0.3106975	1.475262	0.036547	52.892521
223		ICA	0.760624	0.2440691	1.451194	0.037989	56.052682
224		TLBO	0.760809	0.312244	1.47578	0.036551	52.8405
225		GWO	0.760996	0.2430388	1.451219	0.037732	45.116309
226		WCA	0.760908	0.413554	1.504381	0.035363	57.669488

Table A2. Parameters values of the Photowatt-PWP201 module.

Method	Reference	Algorithm	I_{pv} (A)	I_0 (μA)	n	R_S (Ω)	R_P (Ω)
1		GAMNU	1.030766	3.016227	48.09755	1.219119	906.27545
2		GACCC	1.030514	3.482263	48.642835	1.201271	981.98554
3		CPSO	1.0286	8.301	52.243	1.0755	1850.1
4	[26]	EHHO	1.030499	3.488188	48.6428	1.20111	984.49648
5		SGDE	1.0305	3.4823	48.6428	1.20127	981.9822
6		SA	1.0331	3.6642	48.8211	1.1989	833.3333
7		Rcr-IJADE	1.030514	3.482263	48.642835	1.201271	981.98224
8		RLDE	1.0305	3.4823	48.6428	1.2013	981.9823
9		SGDE	1.0305	3.4823	48.6428	1.20127	981.9822
10		IJAYA	1.0302	3.4703	48.6298	1.2016	977.3752
11		SATLBO	1.0305	3.4827	48.6433	1.2013	982.4038
12	[19]	TLBO	1.0305	3.4872	48.6482	1.2011	984.876
13		GWOCS	1.0305	3.465	48.6237	1.2019	982.7566
14		IWOA	1.0305	3.4717	48.6313	1.2016	978.6771
15		MADE	1.0305	3.4823	48.6428	1.2013	981.9823
16		CLPSO	1.0304	3.6131	48.7847	1.1978	1017
17		WHHO	1.030514	3.482109	48.599532000000004	1.201274	981.90523
18		EHHO	1.030583	3.459968	48.575303999999996	1.201853	971.276026
19		JAYA	1.0307	3.4931	48.650399999999998	1.2014	1000
20	[12]	STLBO	1.0305	3.4824	48.639600000000002	1.2013	982.0387
21		TLABC	1.0305	3.4826	48.643200000000000	1.2013	982.1815
22		CLPSO	1.0304	3.6131	48.783600000000000	1.1978	1000
23		BLPSO	1.0305	3.5176	48.679200000000002	1.2002	992.7901
24		DE/BBO	1.0303	3.6172	48.787199999999999	1.1969	1000
25		GSK	1.0305	3.4823	48.6428	1.2013	981.9823
26		ABC	1.0281	4.9125	49.9917	1.1671	990.8662
27		BBO	1.036	3.2658	48.3836	1.2545	994.8378
28		DE	1.0305	3.4823	48.6848	1.2012	981.9823
29		JAYA	1.0304	3.5622	48.7315	1.1967	970.1747
30		PSO	1.0305	3.4258	48.5756	1.2032	971.2958
31		TLBO	1.0306	3.4426	48.5913	1.2027	967.7212
32	[35]	GOTLBO	1.0305	3.5214	48.686	1.1978	984.656
33		ITLBO	1.0305	3.4823	48.6428	1.2013	981.9823
34		RTLBO	1.0305	3.5033	48.666	1.2006	988.5601
35		SATLBO	1.0307	3.3927	48.5435	1.2308	952.6635
36		LETLBO	1.0305	3.4827	48.6522	1.2084	981.9822
37		BSA	1.0306	3.2292	48.3503	1.2118	994.3068
38		TLABC	1.0306	3.4715	48.6313	1.2017	972.9357
39		IWOA	1.0305	3.4218	48.6523	1.2113	983.9964
40		DSO	1.032357	2.496596	47.33406	1.240547	748.32309
41		MPSO	1.03223	2.552134	47.47824	1.23845	762.9058
42		WDOWOAPSO	1.032382	2.512911	47.422944	1.239288	744.71435
43		GCPSO	1.032382	2.512922	47.42298	1.239288	744.71663
44	[13]	TVACPSO	1.031435	2.6386	47.556648	1.235611	821.59514
45		SDA	1.030517	3.481614	48.59892	1.201288	981.59961
46		EHA-NMS	1.030514	3.482263	48.64284	1.201271	981.98225
47		DE-WAO	1.030514	3.482263	48.64284	1.201271	981.98214
48		ABC-TRR	1.030514	3.482263	48.64284	1.201271	981.98223

49	[20]	ISCE	1.030514	3.482263	48.64284	1.201271	981.98228
50		PGJAYA	1.0305	3.4818	48.642372	1.2013	981.8545
51		HFAPS	1.0305	3.4842	48.644892	1.2013	984.2813
52		TLABC	1.03056	3.4715	48.63132	1.20165	972.93567
53		GOFPANM	1.030514	3.482263	48.64284	1.201271	981.98232
54		ORcr-IJAD	1.030514	3.482263	48.64284	1.201271	981.98224
55		(IWAO)	1.0305	3.4717	48.631284	1.2016	978.6771
56		JADE	1.0305	3.48	48.6428	1.2012	981.9823
57		jDE	1.0305	3.48	48.6428	1.2012	981.9823
58		SaDE	1.0305	3.48	48.6425	1.2012	981.899
59		AGDE	1.0305	3.48	48.6428	1.2012	981.9824
60		SHADE	1.0305	3.48	48.6426	1.2012	981.9454
61		SDE	1.0305	3.48	48.6412	1.2013	982.456
62		ITLBO	1.0305	3.48	48.6428	1.2013	981.9824
63		EJADE	1.0305	3.48	48.6428	1.2012	981.9823
64		EGBO	1.0305	3.48	48.6428	1.2013	981.9822
65		JADE	1.0305	3.48	48.6428	1.2012	981.9823

References

1. Abdelkareem, M.A.A.; Eldaly, A.B.M.; Kamal Ahmed Ali, M.; Youssef, I.M.; Xu, L. Monte Carlo sensitivity analysis of vehicle suspension energy harvesting in frequency domain. *J. Adv. Res.* **2020**, *24*, 53–67. https://doi.org/10.1016/j.jare.2020.02.012.
2. Durán-Martín, J.D.; Sánchez Jimenez, P.E.; Valverde, J.M.; Perejón, A.; Arcenegui-Troya, J.; García Triñanes, P.; Pérez Maqueda, L.A. Role of particle size on the multicycle calcium looping activity of limestone for thermochemical energy storage. *J. Adv. Res.* **2020**, *22*, 67–76. https://doi.org/10.1016/j.jare.2019.10.008.
3. Ćalasan, M.; Abdel Aleem, S.H.E.; Zobaa, A.F. On the root mean square error (RMSE) calculation for parameter estimation of photovoltaic models: A novel exact analytical solution based on Lambert W function. *Energy Convers. Manag.* **2020**, *210*, 112716. https://doi.org/10.1016/j.enconman.2020.112716.
4. Askarzadeh, A.; Rezazadeh, A. Extraction of maximum power point in solar cells using bird mating optimizer-based parameters identification approach. *Sol. Energy* **2013**, *90*, 123–133. https://doi.org/10.1016/j.solener.2013.01.010.
5. Ćalasan, M.; Abdel Aleem, S.H.E.; Zobaa, A.F. A new approach for parameters estimation of double and triple diode models of photovoltaic cells based on iterative Lambert W function. *Sol. Energy* **2021**, *218*, 392–412. https://doi.org/10.1016/j.solener.2021.02.038.
6. Araújo, N.M.F.T.S.; Sousa, F.J.P.; Costa, F.B. Equivalent Models for Photovoltaic Cell—A Review. *Rev. Eng. Térmica* **2020**, *19*, 77. https://doi.org/10.5380/reterm.v19i2.78625.
7. Ramadan, A.; Kamel, S.; Taha, I.B.M.; Tostado-Véliz, M. Parameter estimation of modified double-diode and triple-diode photovoltaic models based on wild horse optimizer. *Electron.* **2021**, *10*, 2308. https://doi.org/10.3390/electronics10182308.
8. Rawa, M.; Calasan, M.; Abusorrah, A.; Alhussainy, A.A.; Al-Turki, Y.; Ali, Z.M.; Sindi, H.; Mekhilef, S.; Aleem, S.H.E.A.; Bassi, H. Single Diode Solar Cells—Improved Model and Exact Current–Voltage Analytical Solution Based on Lambert's W Function. *Sensors* **2022**, *22*, 4173. https://doi.org/10.3390/s22114173.
9. Khorami, A.; Joodaki, M. Extracting voltage-dependent series resistance of single diode model for organic solar cells. *SN Appl. Sci.* **2019**, *1*, 619. https://doi.org/10.1007/s42452-019-0613-2.
10. Lekouaghet, B.; Boukabou, A.; Boubakir, C. Estimation of the photovoltaic cells/modules parameters using an improved Rao-based chaotic optimization technique. *Energy Convers. Manag.* **2021**, *229*, 113722. https://doi.org/10.1016/j.enconman.2020.113722.
11. Abdel-Basset, M.; Mohamed, R.; Chakrabortty, R.K.; Sallam, K.; Ryan, M.J. An efficient teaching-learning-based optimization algorithm for parameters identification of photovoltaic models: Analysis and validations. *Energy Convers. Manag.* **2021**, *227*, 113614. https://doi.org/10.1016/j.enconman.2020.113614.
12. Naeijian, M.; Rahimnejad, A.; Ebrahimi, S.M.; Pourmousa, N.; Gadsden, S.A. Parameter estimation of PV solar cells and modules using Whippy Harris Hawks Optimization Algorithm. *Energy Rep.* **2021**, *7*, 4047–4063. https://doi.org/10.1016/j.egyr.2021.06.085.
13. Gnetchejo, P.J.; Ndjakomo Essiane, S.; Dadjé, A.; Ele, P. A combination of Newton-Raphson method and heuristics algorithms for parameter estimation in photovoltaic modules. *Heliyon* **2021**, *7*, e06673. https://doi.org/10.1016/j.heliyon.2021.e06673.
14. El-Fergany, A.A. Parameters identification of PV model using improved slime mould optimizer and Lambert W-function. *Energy Rep.* **2021**, *7*, 875–887. https://doi.org/10.1016/j.egyr.2021.01.093.
15. Ndi, F.E.; Perabi, S.N.; Ndjakomo, S.E.; Ondoua Abessolo, G.; Mengounou Mengata, G. Estimation of single-diode and two diode solar cell parameters by equilibrium optimizer method. *Energy Rep.* **2021**, *7*, 4761–4768. https://doi.org/10.1016/j.egyr.2021.07.025.

16. Houssein, E.H.; Zaki, G.N.; Diab, A.A.Z.; Younis, E.M.G. An efficient Manta Ray Foraging Optimization algorithm for parameter extraction of three-diode photovoltaic model. *Comput. Electr. Eng.* **2021**, *94*, 107304. https://doi.org/10.1016/j.compeleceng.2021.107304.
17. Kumar, C.; Raj, T.D.; Premkumar, M.; Raj, T.D. A new stochastic slime mould optimization algorithm for the estimation of solar photovoltaic cell parameters. *Optik* **2020**, *223*, 165277. https://doi.org/10.1016/j.ijleo.2020.165277.
18. Chen, X.; Yue, H.; Yu, K. Perturbed stochastic fractal search for solar PV parameter estimation. *Energy* **2019**, *189*, 116247. https://doi.org/10.1016/j.energy.2019.116247.
19. Hu, Z.; Gong, W.; Li, S. Reinforcement learning-based differential evolution for parameters extraction of photovoltaic models. *Energy Rep.* **2021**, *7*, 916–928. https://doi.org/10.1016/j.egyr.2021.01.096.
20. Ahmadianfar, I.; Gong, W.; Heidari, A.A.; Golilarz, N.A.; Samadi-Koucheksaraee, A.; Chen, H. Gradient-based optimization with ranking mechanisms for parameter identification of photovoltaic systems. *Energy Rep.* **2021**, *7*, 3979–3997. https://doi.org/10.1016/j.egyr.2021.06.064.
21. Perovich, S.M.; Simic, S.K.; Tosic, D.V.; Bauk, S.I. On the analytical solution of some families of transcendental equations. *Appl. Math. Lett.* **2007**, *20*, 493–498. https://doi.org/10.1016/j.aml.2006.06.008.
22. Perovich, S.M.; Djukanovic, M.D.; Dlabac, T.; Nikolic, D.; Calasan, M.P. Concerning a novel mathematical approach to the solar cell junction ideality factor estimation. *Appl. Math. Model.* **2015**, *39*, 3248–3264. https://doi.org/10.1016/j.apm.2014.11.026.
23. Hashim, F.A.; Hussien, A.G. Snake Optimizer: A novel meta-heuristic optimization algorithm. *Knowl.-Based Syst.* **2022**, *242*, 108320. https://doi.org/10.1016/j.knosys.2022.108320.
24. Suryadi, M.T.; Satria, Y.; Prawadika, L.N. An improvement on the chaotic behavior of the Gauss Map for cryptography purposes using the Circle Map combination. *J. Phys. Conf. Ser.* **2020**, *1490*, 12045. https://doi.org/10.1088/1742-6596/1490/1/012045.
25. Rezk, H.; Inayat, A.; Abdelkareem, M.A.; Olabi, A.G.; Nassef, A.M. Optimal operating parameter determination based on fuzzy logic modeling and marine predators algorithm approaches to improve the methane production via biomass gasification. *Energy* **2022**, *239*, 122072. https://doi.org/10.1016/j.energy.2021.122072.
26. Saadaoui, D.; Elyaqouti, M.; Assalaou, K.; Ben hmamou, D.; Lidaighbi, S. Parameters optimization of solar PV cell/module using genetic algorithm based on non-uniform mutation. *Energy Convers. Manag. X* **2021**, *12*, 100129. https://doi.org/10.1016/j.ecmx.2021.100129.
27. Liu, Y.; Heidari, A.A.; Ye, X.; Liang, G.; Chen, H.; He, C. Boosting slime mould algorithm for parameter identification of photovoltaic models. *Energy* **2021**, *234*, 121164. https://doi.org/10.1016/j.energy.2021.121164.
28. Xiong, G.; Zhang, J.; Shi, D.; Zhu, L.; Yuan, X. Parameter extraction of solar photovoltaic models with an either-or teaching learning based algorithm. *Energy Convers. Manag.* **2020**, *224*, 113395. https://doi.org/10.1016/j.enconman.2020.113395.
29. Gnetchejo, P.J.; Ndjakomo Essiane, S.; Ele, P.; Wamkeue, R.; Mbadjoun Wapet, D.; Perabi Ngoffe, S. Important notes on parameter estimation of solar photovoltaic cell. *Energy Convers. Manag.* **2019**, *197*, 111870. https://doi.org/10.1016/j.enconman.2019.111870.
30. Merchaoui, M.; Sakly, A.; Mimouni, M.F. Particle swarm optimisation with adaptive mutation strategy for photovoltaic solar cell/module parameter extraction. *Energy Convers. Manag.* **2018**, *175*, 151–163. https://doi.org/10.1016/j.enconman.2018.08.081.
31. Wu, L.; Chen, Z.; Long, C.; Cheng, S.; Lin, P.; Chen, Y.; Chen, H. Parameter extraction of photovoltaic models from measured I-V characteristics curves using a hybrid trust-region reflective algorithm. *Appl. Energy* **2018**, *232*, 36–53. https://doi.org/10.1016/j.apenergy.2018.09.161.
32. Beigi, A.M.; Maroosi, A. Parameter identification for solar cells and module using a Hybrid Firefly and Pattern Search Algorithms. *Sol. Energy* **2018**, *171*, 435–446. https://doi.org/10.1016/j.solener.2018.06.092.
33. Rezaee Jordehi, A. Enhanced leader particle swarm optimisation (ELPSO): An efficient algorithm for parameter estimation of photovoltaic (PV) cells and modules. *Sol. Energy* **2018**, *159*, 78–87. https://doi.org/10.1016/j.solener.2017.10.063.
34. Derick, M.; Rani, C.; Rajesh, M.; Farrag, M.E.; Wang, Y.; Busawon, K. An improved optimization technique for estimation of solar photovoltaic parameters. *Sol. Energy* **2017**, *157*, 116–124. https://doi.org/10.1016/j.solener.2017.08.006.
35. Xiong, G.; Li, L.; Mohamed, A.W.; Yuan, X.; Zhang, J. A new method for parameter extraction of solar photovoltaic models using gaining–sharing knowledge based algorithm. *Energy Rep.* **2021**, *7*, 3286–3301. https://doi.org/10.1016/j.egyr.2021.05.030.
36. Ram, J.P.; Babu, T.S.; Dragicevic, T.; Rajasekar, N. A new hybrid bee pollinator flower pollination algorithm for solar PV parameter estimation. *Energy Convers. Manag.* **2017**, *135*, 463–476. https://doi.org/10.1016/j.enconman.2016.12.082.
37. Alam, D.F.; Yousri, D.A.; Eteiba, M.B. Flower Pollination Algorithm based solar PV parameter estimation. *Energy Convers. Manag.* **2015**, *101*, 410–422. https://doi.org/10.1016/j.enconman.2015.05.074.
38. Weng, X.; Heidari, A.A.; Liang, G.; Chen, H.; Ma, X. An evolutionary Nelder–Mead slime mould algorithm with random learning for efficient design of photovoltaic models. *Energy Rep.* **2021**, *7*, 8784–8804. https://doi.org/10.1016/j.egyr.2021.11.019.
39. Jordehi, A.R. Time varying acceleration coefficients particle swarm optimisation (TVACPSO): A new optimisation algorithm for estimating parameters of PV cells and modules. *Energy Convers. Manag.* **2016**, *129*, 262–274. https://doi.org/10.1016/j.enconman.2016.09.085.